Mid-Cretaceous strontium-isotope stratigraphy of deep-sea sections

T. J. Bralower[*]
P. D. Fullagar   *Department of Geology, University of North Carolina, Chapel Hill, North Carolina 27599-3315*
C. K. Paull

G. S. Dwyer   *Department of Geology, Duke University, Durham, North Carolina 27706*

R. M. Leckie   *Department of Geosciences, University of Massachusetts, Amherst, Massachusetts 01003*

ABSTRACT

Large variations exist between published mid-Cretaceous (late Barremian to early Turonian stages) seawater Sr-isotope stratigraphies; this has resulted in disparate interpretations of crustal production rates. We report on a detailed investigation of seawater Sr-isotope stratigraphy based on foraminifers and, where available, on inoceramid bivalves from 12 mid-Cretaceous Deep Sea Drilling Project and Ocean Drilling Program sections. The effects of diagenesis are assessed using scanning electron microscope observations and trace-elemental analyses, but are best distinguished by comparing the $^{87}Sr/^{86}Sr$ values of similar-age samples from different sites. Strontium-isotope analyses compiled from 9 of 12 sites that have detailed age control define one band of common values. This band is used as a composite curve, which presumably represents seawater $^{87}Sr/^{86}Sr$ values. The composite curve shows a "trough" of markedly lower $^{87}Sr/^{86}Sr$ values in the Aptian and early Albian stages, higher but constant values for the middle Albian-Cenomanian stages, followed by a decrease in $^{87}Sr/^{86}Sr$ values in the early Turonian.

Variations between published mid-Cretaceous Sr-isotope records result from diagenetic alteration, analytical problems, and the diverse biostratigraphic approaches and assumptions used to estimate sample ages. When preexisting age data are made consistent, the composite record shows close similarities with data sets derived from measurements of macrofossils in land sections of Europe and North America.

The interval of decreased $^{87}Sr/^{86}Sr$ values in the Aptian-Albian stages overlaps with the pulse of mid-plate volcanic activity that produced the Ontong Java, Manihiki, and Kerguelen Plateaus. The exact age and the shape of the trough, however, are consistent with increased spreading rates at oceanic ridges, given the existing data on the timing of mid-plate volcanic activity.

INTRODUCTION

Major fluctuations in the strontium-isotope composition of seawater are recorded in Phanerozoic marine carbonate strata (e.g., Veizer and Compston, 1974; Brass, 1976; Burke et al., 1982; Hess et al., 1986; McArthur et al., 1993; Jones et al., 1994a). Because the ocean is well mixed with respect to Sr (the residence time of Sr in the oceans is on the order of 10^6 yr and the mixing time of the oceans is on the order of 10^3 yr), and because marine carbonates faithfully record oceanic Sr-isotope ratios at deposition (DePaolo and Ingram, 1985), stratigraphic fluctuations in marine carbonates are assumed to be globally synchronous. For the parts of the time scale where the seawater Sr-isotope curve is confidently established, it can be used to provide age control for other sedimentary rocks and to model geochemical cycles.

Significant advances have been made in the development of a Sr-isotope stratigraphy for the Neogene (e.g., DePaolo and Ingram, 1985; Hodell et al., 1989; Farrell et al., 1995). Because seawater $^{87}Sr/^{86}Sr$ values changed rapidly for much of this time interval, Sr isotopes can be used to date nonfossiliferous or poorly fossiliferous sediments with precision (e.g., Ludwig et al., 1988; McKenzie et al., 1988). Paleogene and Upper Cretaceous Sr-isotope stratigraphies are

also well established (e.g., Denison et al., 1993; McArthur et al., 1993; Sugarman et al., 1995).

The Sr-isotope composition of seawater is controlled largely by variations in the input of Sr from continental weathering, hydrothermal circulation at spreading centers, and from carbonate dissolution. Therefore, changes in Sr-isotope ratios can elucidate the timing of orogenic events and the onset of glaciation (e.g., Raymo et al., 1988; Hodell et al., 1991), and has implications for the extent and timing of ridge-crest and mid-plate volcanism, and possibly even eustasy (e.g., Brass, 1976). Increasing Sr-isotope ratios generally indicate periods during which the supply of continental Sr ($^{87}Sr/^{86}Sr \approx 0.712$) increased with respect to the supply of Sr from mid-ocean ridges ($^{87}Sr/^{86}Sr \approx 0.703$), and conversely decreasing $^{87}Sr/^{86}Sr$ values suggest intervals when volcanic Sr increased with respect to Sr from the continents. Because the absence of magnetic reversals inhibits the dating of oceanic crust of mid-Cretaceous age, Sr-isotope curves have been used on both sides of the debate over the existence of rapid sea-floor spreading in this interval (e.g., Jones et al., 1994b; Ingram et al., 1994; Heller et al., 1996). High mid-Cretaceous crustal production rates at ridge crests and in mid-plate settings are inferred to have been associated with the ascent of a superplume from the mantle (e.g., Larson, 1991; Larson and Kincaid, 1996), a scenario with significant implications (e.g., Hays and Pitman, 1973).

Despite the significance of these data, available Sr-isotope records for the mid-Cretaceous (late Barremian to early Turonian stages) possess great variability. The original studies of Burke et al. (1982) and Koepnick et al. (1985) show a significant amount of internal scatter, largely as a result of diagenetic alteration. Data from more recent studies show far less internal scatter. Pris-

*E-mail: bralower@email.unc.edu

Data Repository item 9752 contains additional material related to this article.

tine remains of Cenomanian-Turonian inoceramids and ammonites from the Western Interior basin of North America were used in the Sr-isotope study of McArthur et al. (1994). Jones et al. (1994b) measured $^{87}Sr/^{86}Sr$ values of original belemnites and oysters obtained from sequences in England, and Ingram et al. (1994) measured Sr-isotope ratios on apatitic remains of fish teeth concentrated from mid-Cretaceous limestone sequences in Italy. Strontium-isotope values of inoceramids from the Albian section of Deep Sea Drilling Project (DSDP) Site 511 on the Falkland Plateau in the South Atlantic were reported by Huber et al. (1995). Jenkyns et al. (1995) measured $^{87}Sr/^{86}Sr$ values on Hauterivian-Albian shallow-water carbonates from Ocean Drilling Program (ODP) Site 866 atop Resolution Guyot in the central Pacific. Large disparities continue to exist between these recent papers. In particular, the Sr-isotope ratios of Ingram et al. (1994) are noticeably higher than those reported by other authors.

The disparities among current mid-Cretaceous Sr-isotope stratigraphies may result from modification of original isotope ratios by diagenetic alteration, or analytical procedures that have sampled Sr from nonbiogenic sources such as clays. Errors also exist in establishing the ages of the samples that come from a geographically diverse set of locations. For example, it is often difficult to correlate precisely between Tethyan and higher latitude sequences, or between sediments deposited in pelagic and shallower water environments.

We present an independent mid-Cretaceous seawater Sr-isotope stratigraphy based on measurements of foraminifers and inoceramids from 12 DSDP and ODP sections. The deep-sea record offers advantages for establishing Sr-isotope stratigraphies: (1) sections are usually more complete than their shallower water counterparts; and (2) cosmopolitan faunal and floral assemblages provide more direct correlation with major tectonic and paleoceanographic events, enabling a thorough analysis of the causes of changes in seawater $^{87}Sr/^{86}Sr$ values.

SITES, SECTIONS, AND METHODS

Sites and Sections

The 12 sites investigated are distributed throughout the major ocean basins (Fig. 1) and include pelagic and hemipelagic depositional settings characterized by nannofossil-rich claystone and chalk (Table 1). The sampled sites compose an expanded, largely continuous, and well-recovered upper Barremian to lower Turonian sequence. Sample spacing averages 1.5 m, equivalent to a temporal duration of about 150 000–250 000 yr at standard sedimentation rates for pelagic carbonates.

Time Control and Correlation

Establishment of Ages and Biostratigraphic Error. Calcareous nannofossil biostratigraphic control exists in all of the sections analyzed and many are also constrained by planktic foraminiferal biostratigraphy (Table 1). Only one site has magnetostratigraphy: basal Aptian magnetic polarity zone M0 was identified at Site 641 (Ogg, 1988).

Chronological ages of all samples are estimated using the integrated calcareous nannofossil-planktic foraminiferal biostratigraphic scheme of Bralower et al. (1993) calibrated to the time scale of Gradstein et al. (1994). The calibration generally follows Premoli Silva and Sliter (1994) and Erba et al. (1996), who calculated planktic foraminiferal and calcareous nannofossil zonal ages from their relative positions in sections from the Umbrian Apennines of Italy assuming constant sedimentation rates. The ages of all datum levels are shown in Figure 2.

Ages of samples in Sites 258, 511, 545, 547, 551, 641 and 763 are estimated by assuming constant sedimentation rates between a series of planktic foraminiferal and nannofossil datum levels (Table 2). We use the most reliable datum levels in each section. Chronological ages of samples from sections that are incomplete or poorly recovered are more difficult to determine. At Sites 390, 392, 417, and 418, only one datum
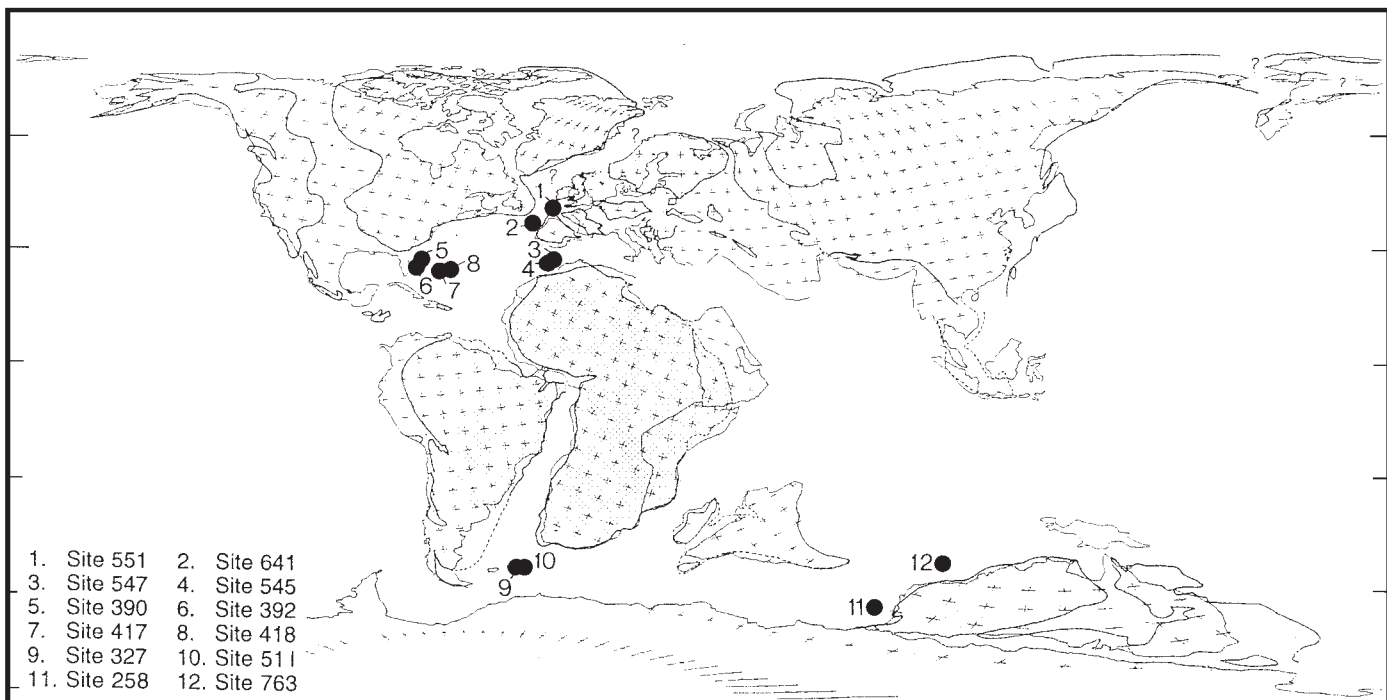

Figure 1. Map showing location of Deep Sea Drilling Project and Ocean Drilling Program sites investigated. The paleogeographic reconstruction for the late Albian stage is after Barron et al. (1981).

TABLE 1. LOCATION, STRATIGRAPHY, LITHOLOGY, AND SOURCES OF BIOSTRATIGRAPHICAL DATA IN SITES INVESTIGATED

Site	Location	Interval	Lithology	Biostratigraphy
DSDP 258	Naturaliste Plateau, Indian Ocean	Upper Albian–Turonian	Light olive-gray nannofossil chalk	Thierstein (1974)(n)
DSDP 327	Falkland Plateau, South Atlantic	Lower Albian	Pink nannofossil chalk	Wise and Wind (1977)(n)
DSDP 390	Blake Nose, North Atlantic	Upper Aptian–lower Albian	Gray-yellow marly nannofossil ooze	Gradstein (1978)(f); Schmidt (1979)(n); this study (n,f)
DSDP 392	Blake Nose, North Atlantic	Barremian–upper Albian	Variable: Light gray-yellow-pink marly nannofossil ooze	Gradstein (1978)(f); Schmidt (1979)(n); this study (n,f)
DSDP 417	Bermuda Rise, North Atlantic	Lower Aptian–upper Albian	Variable: Light gray-brown-pink marly nannofossil ooze	Miles and Orr (1980)(f); Gartner (1980)(n); Siesser (1980); this study (n,f)
DSDP 418	Bermuda Rise, North Atlantic	Upper Aptian–upper Albian	Variable: Pink marly chalk and light gray claystone	Miles and Orr (1980)(f); Gartner (1980)(n); Siesser (1980)(n); this study (n,f)
DSDP 511	Falkland Plateau, South Atlantic	Lower Aptian–upper Cenomanian	Pink nannofossil chalk	Krashenninikov and Basov (1983)(f); Bralower et al. (1993)(f); Wise (1983)(n); Bralower (1992)(n); this study(f)
DSDP 545	Morocco Basin, North Atlantic	Upper Aptian–lower Cenomanian	Light green nannofossil claystone	Leckie (1984)(f); Wiegand (1984)(n); Bralower (1992)(n); this study(f)
DSDP 547	Morocco Basin, North Atlantic	Upper Albian–upper Cenomanian	Green nannofossil claystone	Leckie (1984)(f); Wiegand (1984)(n); Bralower (1992)(n)
DSDP 551	Goban Spur, North Atlantic	Upper Cenomanian–lower Turonian	White nannofossil chalk	Graciansky et al. (1985)(f); Bralower (1988)(n)
ODP 641	Galicia Bank, North Atlantic	Upper Barremian–upper Aptian	Gray nannofossil claystone	Applegate and Bergen (1988)(n); Bralower et al. (1994)(n)
ODP 763	Exmouth Plateau, Indian Ocean	Upper Aptian–lower Turonian	Light green zeolitic nannofossil claystone	Bralower and Siesser (1992)(n); this study (f)

Note: DSDP—Deep Sea Drilling Project, ODP—Ocean Drilling Program, (n)—nannofossils, (f)—foraminifera.

TABLE 2. AGES AND DEPTHS OF NANNOFOSSIL AND PLANKTONIC FORAMINIFERAL DATUM LEVELS IN DSDP/ODP SITES

Datum	Age (Ma)	258	327A	390*	392A[†]	417D[§]	418B[#]	511	545	547	551	641C	763B
Base *Kamptnerius magnificus*	91.8	255.88											
Top *Microstaurus chiastius*	93.5												389.50
Base *Eiffellithus eximius*	93.55										134.30		
Top *Axopodorhabdus albianus*	93.9	263.00									138.77		
Base *Rotalipora cushmani*	96.6									451.90			
Base *Lithraphidites acutum*	96.8								267.18				
Base *Corollithion kennedyi*	97.6									621.96			424.29
Base *Eiffellithus turriseiffelii*	101.7	358.00				297.40**	255.03**	436.42	360.83	757.81			457.80
Base *Rotalipora ticinensis*	101.7												
Base *Biticinella breggiensis*	105.0				81.03**								
Base *Axopodorhabdus albianus*	106.1												486.32
Base *Tranolithus orionatus*	107.3							447.43					494.28
Base *Ticinella primula*	109.5			149.54**									
Base *Sollasites falklandensis*	111.44		313.59**††										
Top *Ticinella bejaouaensis*	112.4								390.75				
Base *Prediscosphaera columnata*	112.6					318.13**							528.75
Top *Planomalina cheniourensis*	112.6				82.31**								
Base *Ticinella bejaouaensis*	114.3							490.50	464.83				
Top *Globigerinellodes algerianus*	115.2			154.13**					490.43				
Base *Globigerinelloides algerianus*	117.1								518.04				
Base *Globigerinelloides ferreolensis*	118.2								523.76				
Base *Eprolithus floralis*	119.0					337.70		510.90				222.70	
Base *Rucinolithus irregularis*	121.0											248.70	

Note: DSDP—Deep Sea Drilling Project, ODP—Ocean Drilling Program, FO—first occurrence, LO—last occurrence.

*,[†],[§],[#]Foraminiferal biostratigraphy of these sites is revised after Gradstein (1978) and Miles and Orr (1980).

*Sample 5-1, 116 cm, is placed in the middle part of the *Planomalina cheniourensis* subzone of the *Ticinella bejaouaensis* zone on the basis of the presence of both nominate taxa. Sample 5-2, 101 cm, lies in the uppermost part of the *Globigerinelloides algerianus* zone. The FO of *Ticinella primula* lies between samples 4-CC and 5R-1, 88 cm.

[†]FO of *Biticinella breggiensis* (middle-upper Albian boundary) is placed between samples 3-1, 94 cm, and 3-2, 102 cm. The LO of *P. cheniourensis* lies between samples 3-2, 102 cm, and 3-3, 70 cm.

[§]Cores 19 and 20 are placed in the basal Albian *Hedbergella planispira* zone based on the presence of *"Globigerinelloides" gyroidinaeformis* and the absence of *T. bejaouaensis* and *T. primula*. Core 17 lies in the upper Albian *Rotalipora ticinensis* zone based on the presence of *R. ticinensis*, and absence of *R. appenninica*.

[#]Samples in core 32 are placed in the lower part of the uppermost Aptian *T. bejaouaensis* foraminiferal zone based on the presence of the nominate taxon, *Hedbergella trocoidea*, *"Globigerinelloides" gyroidinaeformis,* specimens belonging to the *G. blowi* group, the nannofossils *Eprolithus floralis* and *Parhabdolithus achlyostaurion,* and the absence of the foraminifers *Globigerinelloides algerianus*, *G. ferreolensis,* and *G. aptiense,* and the nannofossil *Prediscosphaera columnata*. Core 33 is placed in the middle of the lower upper Aptian *Leupoldina cabri* zone based on the presence of the foraminifer *G. blowi* and the nannofossil *E. floralis*, but absence of the foraminifers *G. algerianus* and *G. ferreolensis*.

**A sedimentation rate of 5 m/m.y. is used to calculate ages of samples from these datum levels.

[††]This datum level is assumed to lie close to the base of core 327A-21 on the basis of a comparison of the ranges of the *S. falklandensis, P. columnata*, and *T. orionatus* at nearby Site 511.

Figure 2 chronostratigraphic chart

AGE Ma	AGE	MAGNETIC CHRON	FORAMINIFER ZONE	SUBZONE	NANNOFOSSIL ZONE	SUBZONE
92	TURONIAN		M. sigali		K. magnificus (NC14)	
			H. helvetica		E. floralis (NC13*)	
94			W. archaeo.		P. asper (NC12*)	E. eximius / M. chiastius
96	CENOMANIAN		R. cushmani	D. algeriana / R. greenhornensis	L. acutum (NC11)	
			R. reicheli			
98			R. brotzeni		E. turriseiffelii (NC10)	NC10B / NC10A
100			R. appenninica			
			R. ticinensis			
102	L		B. breggiensis	subticinensis / praeticinensis	A. albianus (NC9)	NC9B / NC9A
104		C34N				
106	M		T. primula		P. columnata (NC8)	NC8C / NC8B / NC8A
108						
110	E		H. planispira			
112			T. bejaouaensis	T. roberti / P. cheniour.	P. angustus (NC7)	NC7C / NC7B / NC7A
114	L		H. trocoidea			
116	APTIAN	ISEA	G. algerianus			
118		C34N	G. ferreolensis / L. cabri		C. litterarius (NC6)	NC6B / NC6A
120	E	CMO	G. blowi			
122	BARREMIAN	CM1n			W. oblonga (NC5)	NC5E
124		CM1				

NANNO/FORAM BIOHORIZON

- top H. helvetica (90.7)
- **base K. magnificus (91.8)**
- **top P. asper (92.9)**
- base H. helvetica (93.0)
- **top M. chiastius (93.5)**
- **top A. albianus (93.9)**
- top R. cushmani (94.0)
- base D. algeriana (95.4)
- base R. cushmani (96.6)
- base R. reicheli (96.8)
- **base L. acutum (96.8)**
- **base C. kennedyi (97.6)**
- base R. brotzeni (98.9)
- base R. appenninica (100.4)
- base R. ticinensis (101.7)
- **base E. turriseiffelii (101.7)**
- base R. subticinensis (102.4)
- base B. breggiensis (105.0)
- **base E. cf. E. eximius (105.0)**
- **base A. albianus (106.1)**
- **base T. orionatus (107.3)**
- base T. primula (109.5)
- **base H. albiensis (110.9)**
- base low diversity
- top T. bejaouaensis (112.4)
- **base P. columnata (112.6)**
- top P. cheniourensis (112.6)
- base T. bejaouaensis (114.3)
- **base P. achlyostaurion (115.2)**
- top G. algerianus (115.2)
- base G. algerianus (117.1)
- **top M. hoschulzii (117.3)**
- top L. cabri (118.2)
- **base E. floralis (119.0)**
- base L. cabri (119.2)
- **top C. rothii (119.5)**
- **base R. irregularis (121.0)**

Figure 2. The chronostratigraphic scheme utilized in this study. Integrated nannofossil and planktic foraminiferal zonation is after Bralower et al. (1993), calibrated to the time scale of Gradstein et al. (1994), following Premoli Silva and Sliter (1994) and Erba et al. (1996). Ages of the Aptian nannofossil subzonal datum levels are estimated directly from their correlation with foraminiferal datum levels or stage boundaries where they correlate closely. In the Albian stage, where the sections studied by Premoli Silva and Sliter (1994) appear to be condensed, the ages of nannofossil subzonal datum levels are calculated from their relative positions between the first occurrences of *Prediscosphaera columnata* and *Eiffellithus turriseiffelii* in the expanded and apparently complete Albian section at Ocean Drilling Program Site 763 (from Bralower and Siesser, 1992), assuming constant sedimentation rates.

can be accurately determined in any continuous stratigraphic interval. Here a constant sedimentation rate of 5 m/m.y. above and below this datum is assumed, a rate typical for Holocene calcareous oozes from the North Atlantic (Berger, 1974). The major source of error in determining the ages of samples is associated with the assumption of constant sedimentation rates. This error is significantly larger in sections that are incompletely recovered, because datum levels cannot be placed precisely. In these cases the magnitude of the potential error approaches the duration of the zonal unit of interest, although we believe that the errors are much less than this.

Correlation with Previous Sr-Isotope Stratigraphies. Our calculated sample ages enable correlation with previously published Sr-isotope stratigraphies based on macrofossil biostratigraphy (McArthur et al., 1994; Jones et al., 1994b) after these data sets were recalibrated to the Gradstein et al. (1994) time scale. The sections investigated by Ingram et al. (1994) have planktic foraminiferal biostratigraphic control allowing direct comparison with the chronostratigraphic scheme derived here (Fig. 2). Samples analyzed by Ingram et al. (1994) were calibrated to the Harland et al. (1989) time scale, but the data of Koepnick et al. (1985), which they incorporated, appear to have remained correlated to the Harland et al. (1982) time scale. In addition, the biostratigraphy of samples from Site 167 in Koepnick et al. (1985) was taken from Winterer et al. (1973) and modifications to the biostratigraphy of this site by Tarduno et al. (1989) resulted in changes in chronological ages of as much as 10 m.y. To compare the Ingram et al. (1994) stratigraphy with other data, we have recalibrated the Koepnick et al. (1985) ages to the Gradstein et al. (1994) time scale by (1) using the revised planktic foraminifer biochronology of Site 167 from Tarduno et al. (1989), and (2) assuming similar relative stage positions for the ages given by Koepnick et al. (1985) for the Iranian samples.

Sample Preparation

Although different processing techniques are used to extract foraminifers for Sr-isotope analyses (e.g., Hodell et al., 1989; DePaolo and Finger, 1991; Sugarman et al., 1995), we avoided use of chemicals such as Calgon and kerosene to break up material because of uncertain effects on the Sr-isotope ratios. About 5 cm^3 of material was broken into pea-sized pieces in a pestle and mortar. These pieces were soaked in pH-9 buffered, deionized water with 10% H_2O_2, and then placed on a shaker table overnight. The residue was passed through 250, 125, and 63 µm sieves with buffered, deionized water. Material

remaining on the sieves was washed onto filter papers and dried in a 60 ºC oven.

Foraminifers were picked for isotope analysis using a binocular microscope. No distinction was made between planktic and benthic foraminifers. Where available, approximately 50 of the best preserved specimens regardless of taxonomic category were picked from the >250 µm fraction; if this size fraction contained an inadequate number of foraminifers, as many as 150 specimens were separated from the 125–250 µm fraction. Only in the upper Barremian–lower Aptian interval of Site 641 was it necessary to pick the foraminifers from the 63–125 µm fraction. Where other fossil material was present, e.g., ostracodes or inoceramids, several fragments were isolated for separate Sr-isotope measurements. A few bulk carbonate Sr-isotope analyses were carried out at Site 763.

The degrees of overgrowth and infilling of foraminifers were noted in each sample. To document preservation further, two typical foraminiferal specimens from each sample were observed in a Leica Stereoscan 440 scanning electron microscope (SEM) at the University of North Carolina–Chapel Hill. Several samples of variable external preservation were broken open to observe the interior of the chambers. Energy dispersive X-ray spectrometry was used to identify nonskeletal mineral phases.

Strontium-Isotope Analysis

Samples were dissolved in 500 µL of 1 M acetic acid, centrifuged, and the decantate was dried. The sample was then dissolved in 250 ml of 5 N HNO_3, loaded on a column containing 50 µl of Eichrom SrSpec resin, washed with 750 µl of 5 N HNO_3, and the Sr was collected in 1 ml of H_2O. Total procedural blanks were 100 to 200 pg. Small samples (0.2–1 mg) were loaded in $TaCl_5$ on single Re filaments; larger samples (1–5 mg) were loaded on single Ta filaments. Samples were analyzed at the University of North Carolina–Chapel Hill on a VG Sector 54 thermal ionization mass spectrometer in dynamic mode. Fractionation is corrected using $^{86}Sr/^{88}Sr = 0.1194$. Strontium-isotope values are archived in Table DR1.[1]

During this study, $^{87}Sr/^{86}Sr$ analyses of 330 aliquots of Sr carbonate standard SRM987 yielded an average value of 0.710246 ± 34 (2σ). Part of this uncertainty is the result of degradation of the collectors used to measure the relative intensity of the Sr ion beams. In fact, some collectors were replaced twice during the course of this

---

[1]GSA Data Repository item 9752, a table of strontium-isotope values, is available on request from Documents Secretary, GSA, P.O. Box 9140, Boulder, CO 80301; e-mail: editing@geosociety.org.

study. To minimize instrumental variation, we analyzed three to six, usually five, SRM987 aliquots in each sample carousel, and used the values obtained to adjust the $^{87}Sr/^{86}Sr$ ratios of the samples. We accepted 0.710250 as the correct $^{87}Sr/^{86}Sr$ value of SRM987. If, for example, the values for the standards in a particular turret averaged 0.710246, we added 0.000004 to the $^{87}Sr/^{86}Sr$ ratio for each sample. This procedure reduced the uncertainty for all 330 analyses of SRM987 to ±25 (2σ). We analyzed 28 samples in duplicate (see footnote 1); for 90% of these samples, the individual $^{87}Sr/^{86}Sr$ ratios were within ±15 of the mean of the duplicate analyses. Internal precision for Sr-isotope analysis was typically 0.0006% to 0.0009% standard error, based on 100 dynamic cycles of data collection.

Tests were conducted to estimate variations in $^{87}Sr/^{86}Sr$ values of the utilized fossil materials. Different foraminiferal fractions from the same sample (combined planktics and benthics of all size fractions, combined planktics and benthics >250 µm, separate planktics, separate benthics) show negligible differences in $^{87}Sr/^{86}Sr$ values (Fig. 3), justifying our measurement of mixed foraminifers.
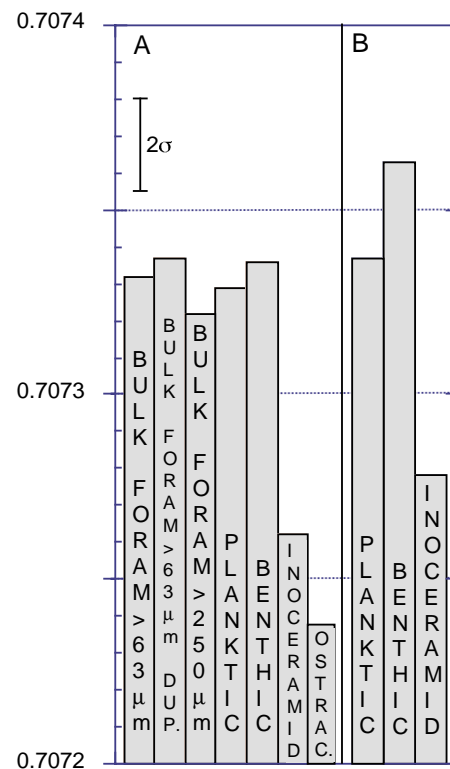

Figure 3. Comparison of $^{87}Sr/^{86}Sr$ values of different fossil components in samples from Site 511. (A) Sample 511-56-3, 43–45 cm. (B) Sample 511-55-3, 39–41 cm. Bulk foram—combined benthics and planktics; Dup.—duplicate analysis; Ostrac.—ostracods.

Trace Elemental Analysis

To evaluate further the extent of postdepositional alteration of the samples, we determined trace- and minor-element:calcium ratios on representative splits of foraminifers and inoceramid prisms (where present) from carefully selected samples from all sites except Site 258. Samples were dissolved in 0.5 N nitric acid and analyzed for their Ca, Mg, Sr, Na, Fe, Mn, and Ba content on a Fisons Spectraspan 7 direct current plasma atomic emission spectrophotometer at the Department of Geology, Duke University. Matrix-matched instrument-calibration standards were prepared from Spex brand pure, single-element plasma-grade solutions. An internal consistency standard prepared from an in-house limestone standard (PE3) and plasma-grade solutions was analyzed repeatedly to monitor run-to-run precision. On the basis of these repeated analyses of standard PE3, precision for Mg/Ca, Sr/Ca, Mn/Ca, and Ba/Ca ratios is better than $\pm 4\%$ (2σ), whereas precision for Na/Ca and Fe/Ca ratios is better than $\pm 8\%$. Trace-elemental data are compiled in Table DR1 (see footnote 1).

RESULTS

Foraminiferal Preservation

Light microscope observations indicate that foraminifer preservation is variable between sites and within individual sections. Scanning electronic microscope (SEM) inspection of the wall texture and chamber filling suggests that, in many cases, light microscopic observations are unsuitable for evaluating the diagenetic alteration of the foraminifers analyzed. For example, specimens from Site 547 which possess a nearly pristine wall texture and appear translucent in the light microscope are filled with sparry calcite or other authigenic mineral phases. Conversely, foraminifers from Site 641 that appear to be poorly preserved in the light microscope are nearly hollow and have only slightly overgrown wall textures. Foraminiferal preservation in the sites investigated is summarized in Table 3. Figure 4 illustrates SEM micrographs of specimens showing the complete range of preservation observed. More detailed illustrations of foraminiferal preservation are given in Fassell and Bralower (in press).

Strontium-Isotope Data

Site 511. Strontium-isotope ratios of foraminifers and inoceramids show similar stratigraphic trends for most of the section studied at Site 511 (Fig. 5). Foraminiferal [87]Sr/[86]Sr values increase from close to 0.707250 near the base of

nannofossil zone NC8 (480 m below sea floor [mbsf]) to close to 0.707450 at the base of zone NC9 (445 mbsf), and decrease slightly in zones NC9 and NC10 (435 mbsf) (Fig. 5). Strontium-isotope ratios measured on inoceramids have slightly less inter-sample variability, and have average values that are 0.000016 lower than the foraminifers. Between 493 and 481 mbsf, trends are different, and inoceramids record values of as much as 0.0001 lower (Fig. 5).

Site 545. Considerable intersample variability exists in [87]Sr/[86]Sr values in zone NC7 and the lower part of zone NC8 (420–530 mbsf) (Fig. 6). Values appear to decrease upward from 0.70745 at 530 mbsf to 0.7073 at 515 mbsf. Strontium-isotope values fluctuate around 0.7073 from 515 to 420 mbsf. Values increase markedly between 390 and 375 mbsf across the unconformity between zones NC8 and NC9; the abrupt increase apparently results from mixing of foraminifers of different ages in a slump in core 40. Thus Sr-isotope measurements from this core were excluded from subsequent analysis. Strontium-isotope values remain close to 0.70745 and show less variability in zone NC10 and the lower part of zone NC11 (360 to 260 mbsf).

Site 547. The [87]Sr/[86]Sr values of foraminifers at Site 547 show few consistent long-term trends (Fig. 7). Samples between 780 and 740 mbsf tend to have higher values (approximately 0.70755) than those above 700 mbsf, where values fluctuate between 0.70730 and 0.70755.

Hole 763B. The biostratigraphically complete upper Aptian to lower Turonian section at Site 763 records no long-term trends in [87]Sr/[86]Sr values measured on foraminifers (Fig. 8). Instead, this section shows 2–20 m 0.0001–0.0003 amplitude, multisample fluctuations. Bulk and inoceramid [87]Sr/[86]Sr values are predominantly higher than those measured on foraminifers in the same samples.

Other Sites. Strontium-isotope measurements of samples from Sites 258, 327, 390, 392, 417, 418, 551, and 641 are illustrated in Figures 9–16. In general, considerably less intersample variability is observed within individual nannofossil zones than between zones. Inoceramid [87]Sr/[86]Sr values are slightly lower than those measured on foraminifers (Figs. 10 and 12).

DISCUSSION

Monitoring Diagenesis of Samples

The Sr-isotope composition of pore waters of marine sediments may be different from the carbonates with which they are associated (Elderfield and Gieskes, 1982; Richter and DePaolo, 1988; Paull et al., 1995), and recrystallization may lead to altered Sr-isotope ratios. However, the presence of secondary calcite does not necessarily signify diagenetically altered Sr-isotope ratios, because the Sr in the diagenetic calcite may be obtained from local dissolution (e.g., Jenkyns et al., 1995). Even small amounts

TABLE 3. SUMMARY OF FORAMINIFERAL PRESERVATION

Site	Description	Illustrations
DSDP 258	Wall texture well preserved; many specimens are hollow, few are filled with calcite. Rarely chambers filled with loosely packed sub-micron sized lepispheres of opal-CT and long bladed crystals of zeolite.	Plate 5[†]
DSDP 327	Well preserved in sections 21-1 and 21-2; slightly infilled with calcite in sections 21-3 and 21-4.	Figure 4g*, Plate 1[†]
DSDP 390	Specimens hollow, outer and inner walls slightly overgrown, and pores partly infilled.	Plate 3[†]
DSDP 392	Outer and inner wall texture of certain foraminifers slightly overgrown, inner wall structure appears to be nearly pristine in most specimens.	Figure 4, c and d*, Plate 2[†]
DSDP 417	Specimens hollow, outer and inner walls slightly overgrown, and pores partly infilled.	Plate 3[†]
DSDP 418	Specimens hollow, outer and inner walls slightly overgrown, and pores partly infilled.	Plate 3[†]
DSDP 511	Almost all benthic and planktic specimens hollow. Above core 55: pristine wall structure. Core 55 and below: infilling of pores and some chambers. Inoceramid preservation excellent.	Figure 4, a and f*, Plate 1[†]
DSDP 545	Outer and inner walls of many specimens overgrown by calcite, most pores are infilled. Chamber centers range from hollow to infilled with sparry calcite	Plate 5[†]
DSDP 547	Most specimens possess almost unaltered wall structure with only partial pore infilling. Most chambers entirely infilled with sparry calcite	Figure 4, j, k, and l*, Plate 4[†]
DSDP 551	Specimens hollow, outer and inner walls slightly overgrown, and pores partly infilled.	Figure 4b*, Plate 3[†]
ODP 641	Slightly overgrown wall texture, minor to moderate amount of calcite chamber filling.	Figure 4, e and h*, Plate 2[†]
ODP 763	Wall texture well preserved; many specimens are hollow, few are filled with calcite. Commonly chambers almost entirely filled by loosely packed submicron-sized lepispheres of opal-CT and long bladed crystals of zeolite.	Figure 4i*, Plate 6[†]

Note: DSDP—Deep Sea Drilling Project, ODP—Ocean Drilling Program.
*This paper.
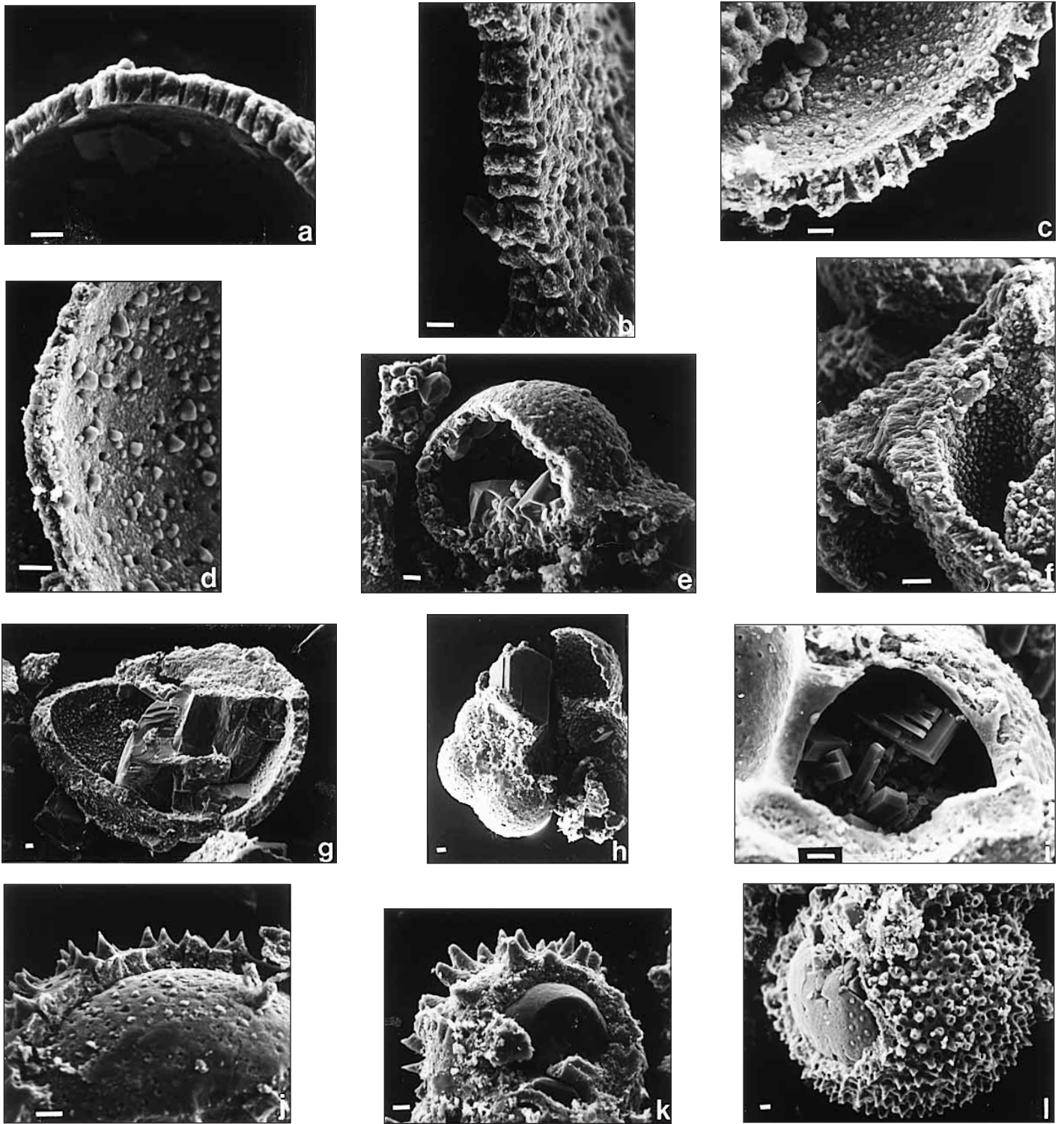[†]Fassell and Bralower (in press).

Figure 4. (a) Sample 511-51-6, 12–14 cm, wall structure shows unfilled pores. (b) Sample 551-5-1, 91–94 cm, wall structure shows minor overgrowth. (c) Sample 392A-3-1, 86–88 cm, wall shows minor overgrowth on inside, but little pore infilling. (d) Sample 392A-2-2, 109–112 cm, wall shows moderate overgrowth on inside. (e) Sample 641C-10R-1, 87–89 cm, broken specimen shows rhombs of calcite growing inside chamber. (f) Sample 511-55-2, 15–17 cm, moderately overgrown wall texture. (g) Sample 327A-21-3, 133–136 cm, inside of a chamber shows calcite infilling. (h) Sample 641C-11R-2, 3–6 cm, broken planktic specimen shows overgrown outer wall and rhomb of calcite lodged inside. (i) Sample 763B-35X-5, 33–40 cm, broken specimen shows slightly overgrown wall and chamber infilling of zeolite (large blady crystals), coccoliths, and minute cristobalite lepispheres. (j, k) Sample 547A-54-2, 26–29 cm, broken specimen shows entirely infilled chamber and overgrown spines in photo k. (l) Sample 547A-45-2, 34–37 cm, broken specimen of *Hedbergella* sp. shows entirely infilled chamber, pristine wall and incipient pore infilling. Scale bars represent 5 µm. See Table 3 for summary of preservation of sites.
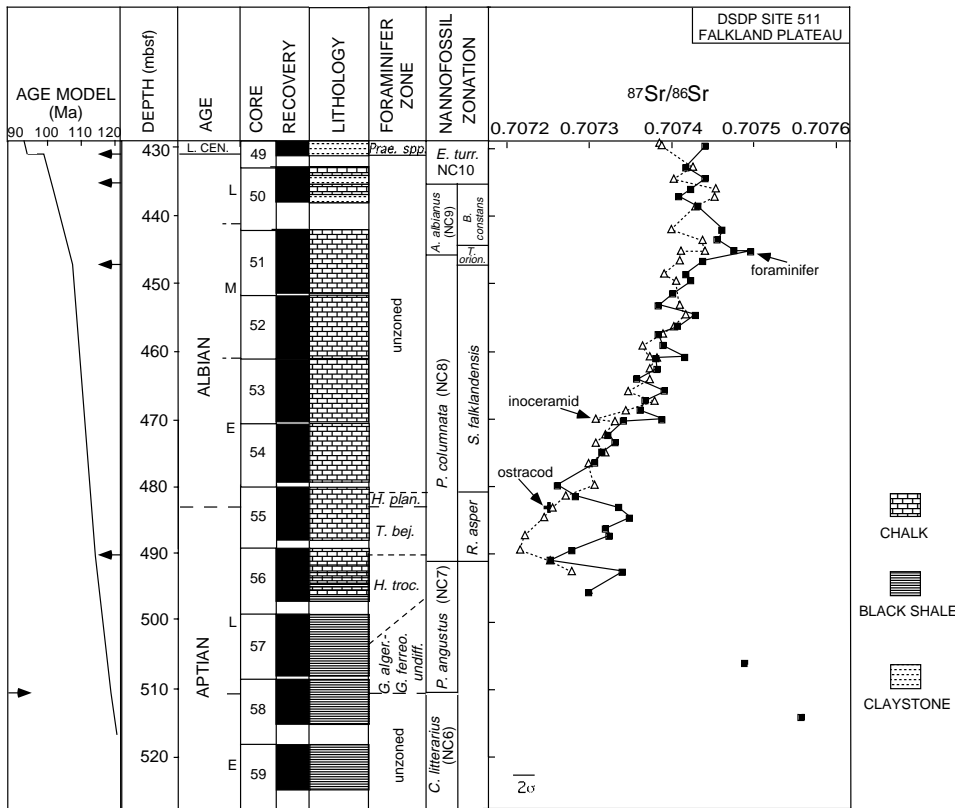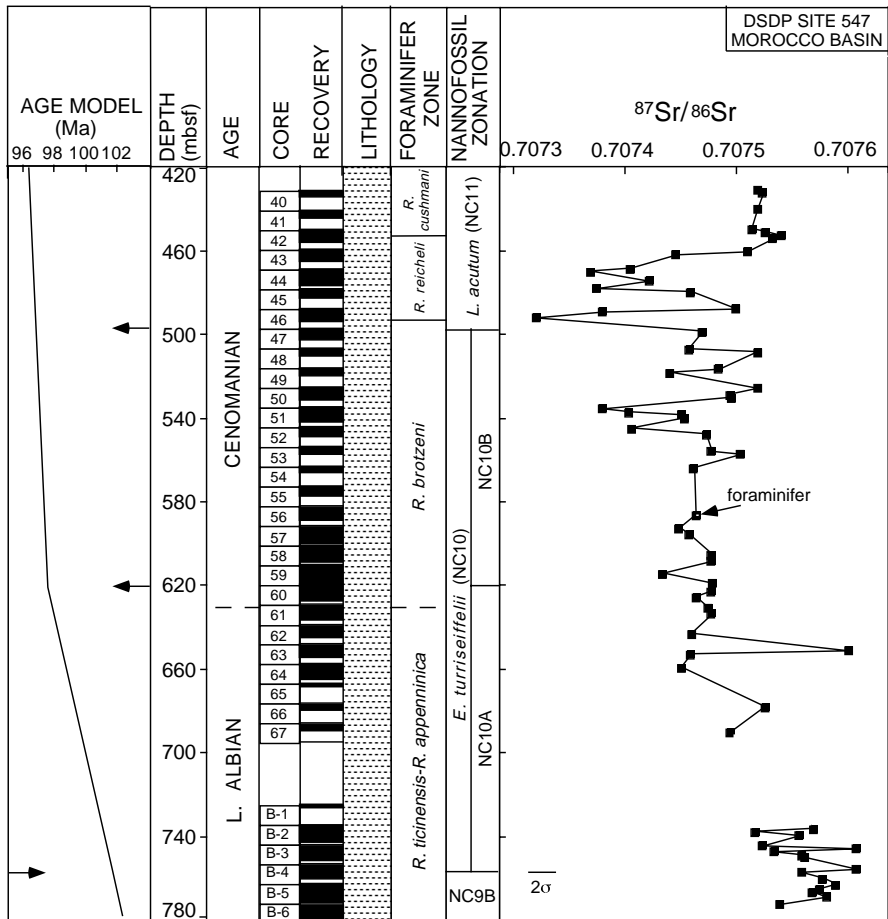
Figure 5. Strontium-isotope data from Site 511. Nannofossil biostratigraphy is after Wise (1983), modified by Bralower (1992). Planktic foraminiferal biostratigraphy is modified after Bralower et al. (1993). An age model is shown on the left; arrows signify tie points (see Table 2). The base of core 49 is placed in the upper Cenomanian stage, following Krasheninnikov and Basov (1983). Cen—Cenomanian, mbsf—meters below sea floor.
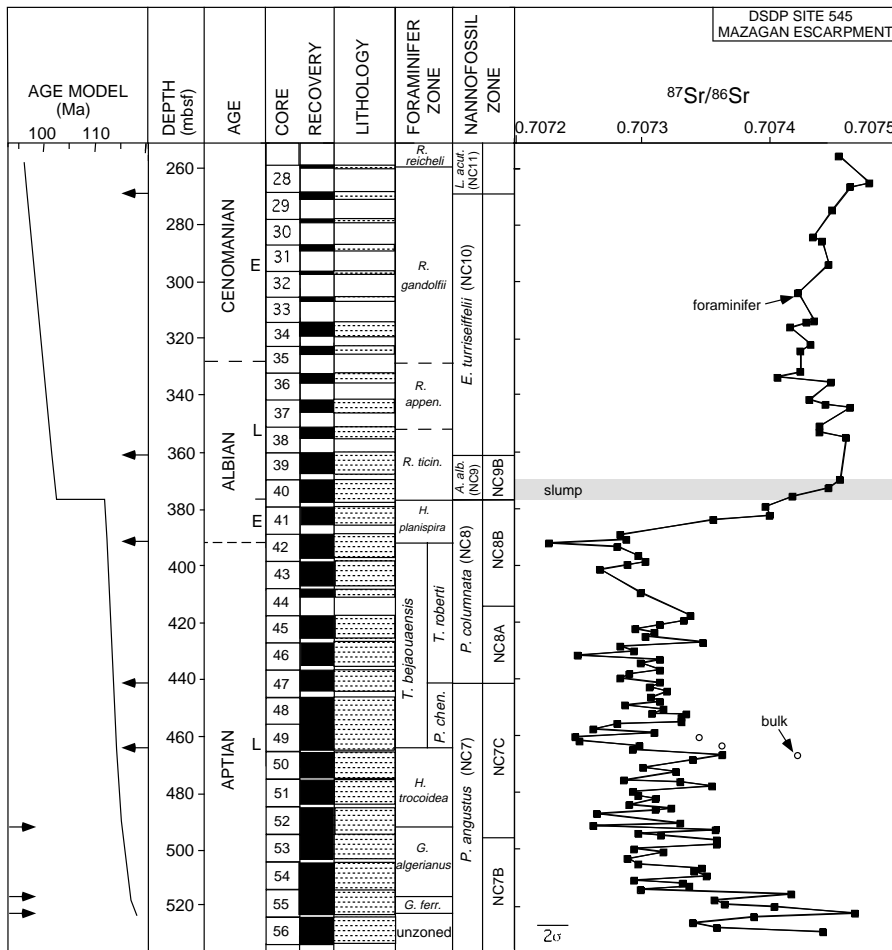
Figure 6. Strontium-isotope data from Site 545. The nannofossil biostratigraphy is after Wiegand (1984), modified by Bralower (1992). The planktic foraminiferal biostratigraphy is modified after Leckie (1984). The position of the slump is indicated. An age model is shown on the left; arrows signify tie points (see Table 2). The key to the lithologic column is given in Figure 5. mbsf—meters below sea floor.

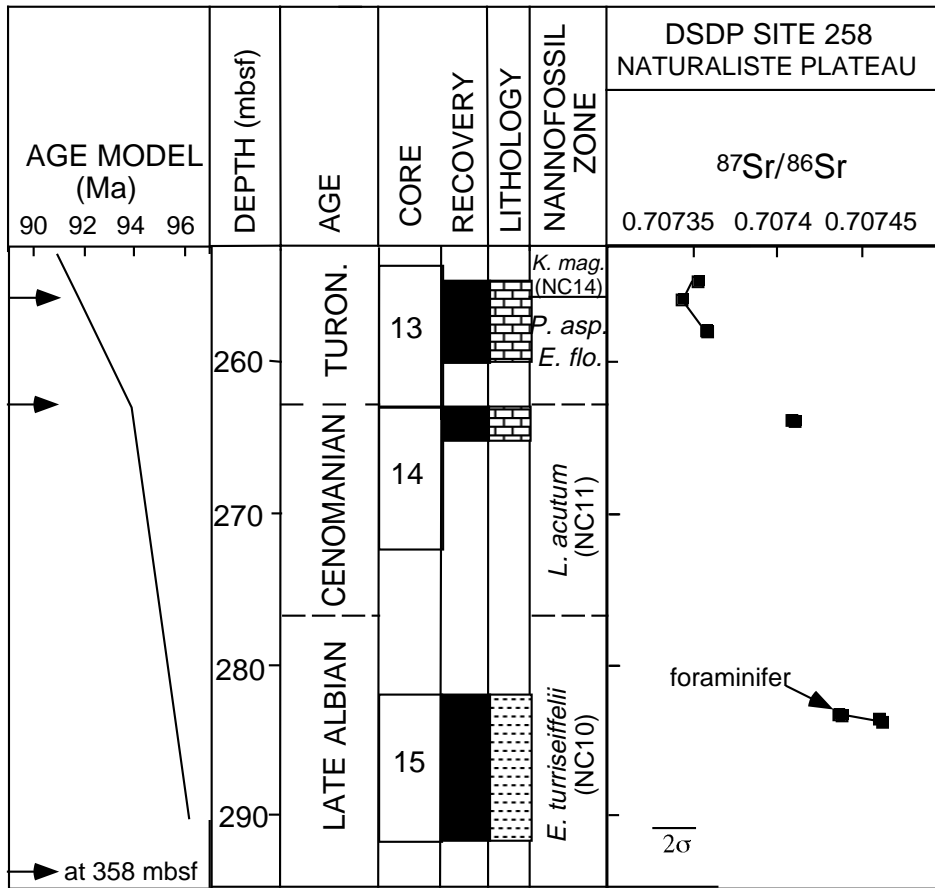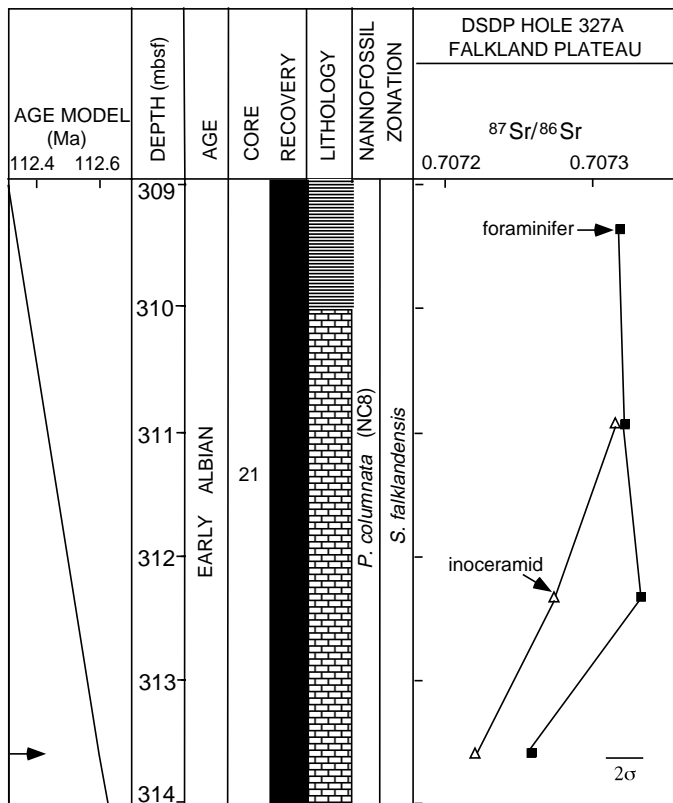**Figure 7. Strontium-isotope analyses of foraminifers from Site 547. Nannofossil biostratigraphy is after Wiegand (1984), modified by Bralower (1992). The planktic foraminiferal biostratigraphy is after Leckie (1984). An age model is shown on the left; arrows signify tie points (see Table 2). The key to the lithologic column is given in Figure 5. mbsf—meters below sea floor.**
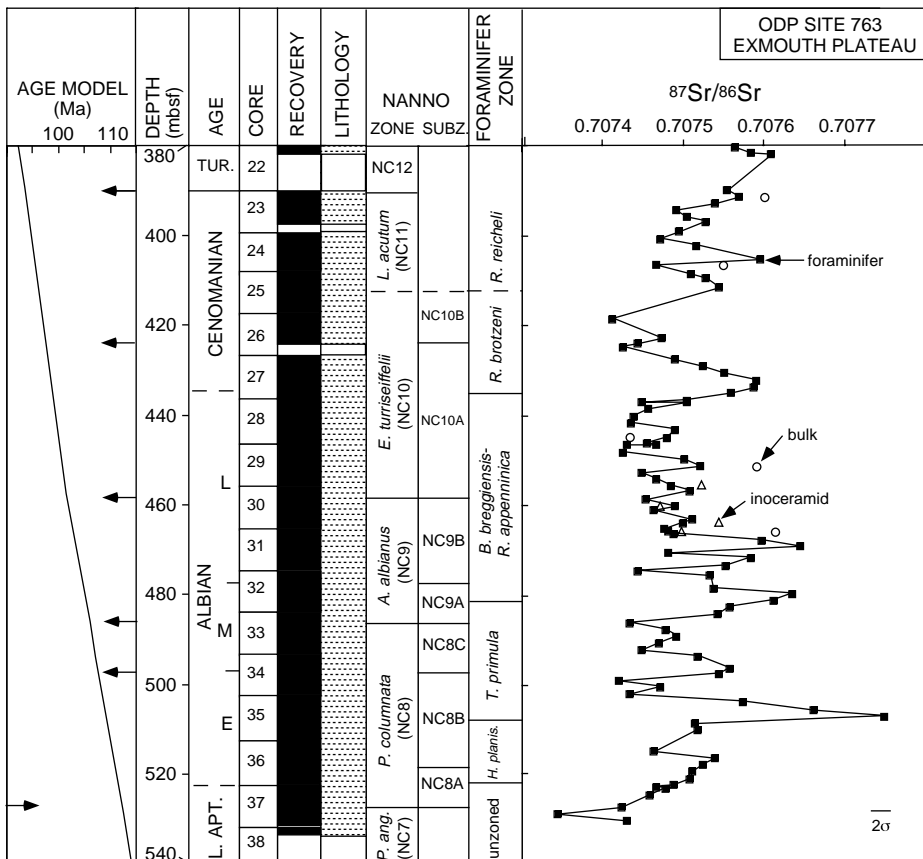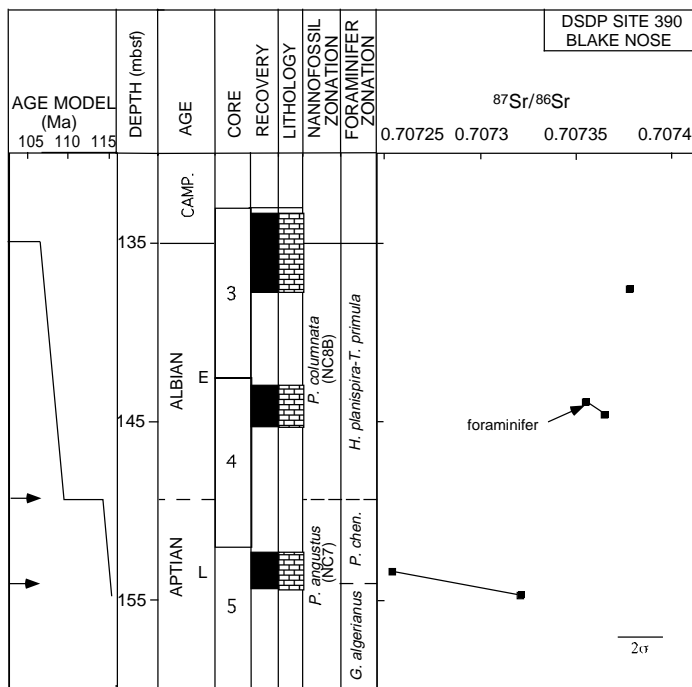
Figure 8. Strontium-isotope data from Hole 763B. The nannofossil biostratigraphy is after Bralower and Siesser (1992). Planktic foraminiferal biostratigraphy is from this study. An age model is shown on the left; arrows signify tie points (see Table 2). The key to the lithologic column is given in Figure 5. Tur.—Turonian, mbsf—meters below sea floor.

Figure 9. Strontium-isotope analyses of foraminifers from Site 258. The nannofossil biostratigraphy is after Thierstein (1974). An age model is shown on the left; arrows signify tie points (see Table 2). The key to the lithologic column is given in Figure 5. Turon.—Turonian, mbsf—meters below sea floor.

Figure 10. Strontium-isotope data from Hole 327A. The nannofossil biostratigraphy is after Wise and Wind (1977). An age model is shown on the left; the arrow signifies tie point (see Table 2). The key to the lithologic column is given in Figure 5. mbsf—meters below sea floor.

Figure 11. Strontium-isotope analyses of foraminifers from Site 390. The nannofossil biostratigraphy is after Schmidt (1979), modified as part of this study. Planktic foraminiferal biostratigraphy is modified after Gradstein (1978). An age model is shown on the left; arrows signify tie points (see Table 2). The key to the lithologic column is given in Figure 5. Camp.—Campanian, mbsf—meters below sea floor.
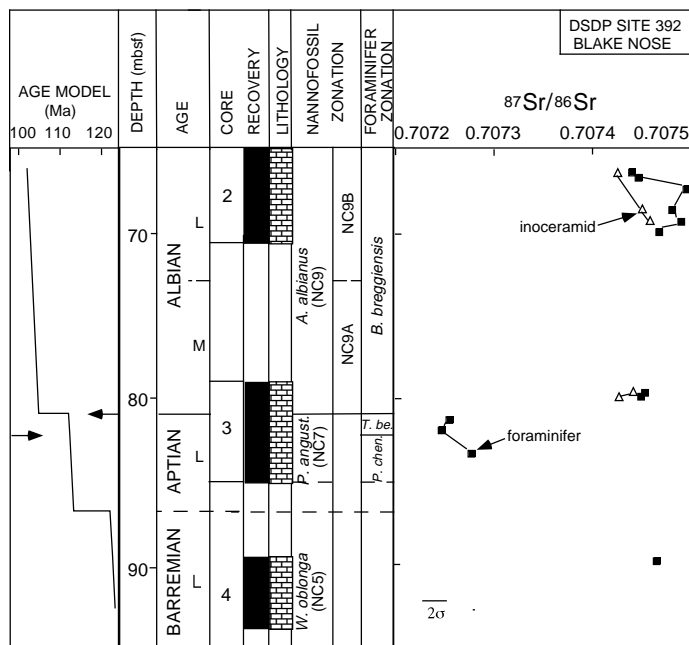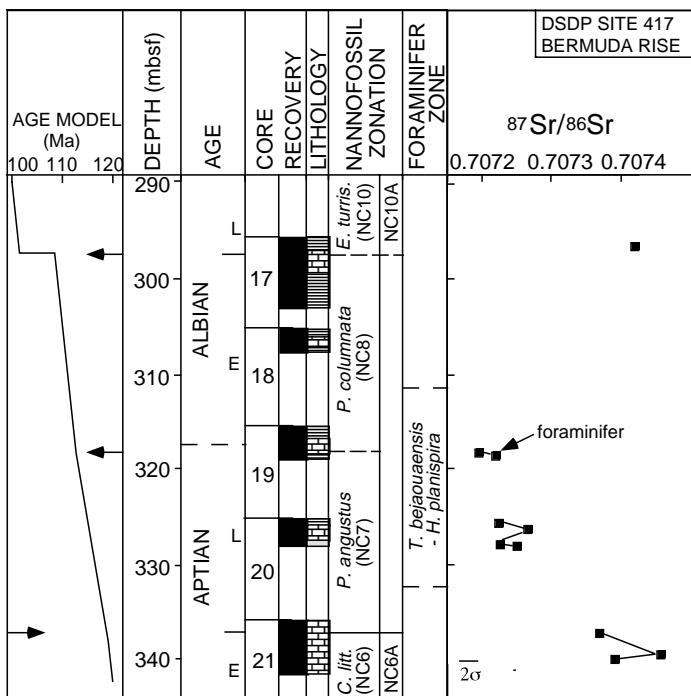

Figure 12. Strontium-isotope data from Hole 392A. The nannofossil biostratigraphy is after Schmidt (1979), modified as part of this study. Planktic foraminiferal biostratigraphy is modified after Gradstein (1978). An age model is shown on the left; arrows signify tie points (see Table 2). The key to the lithologic column is given in Figure 5; mbsf—meters below sea floor.
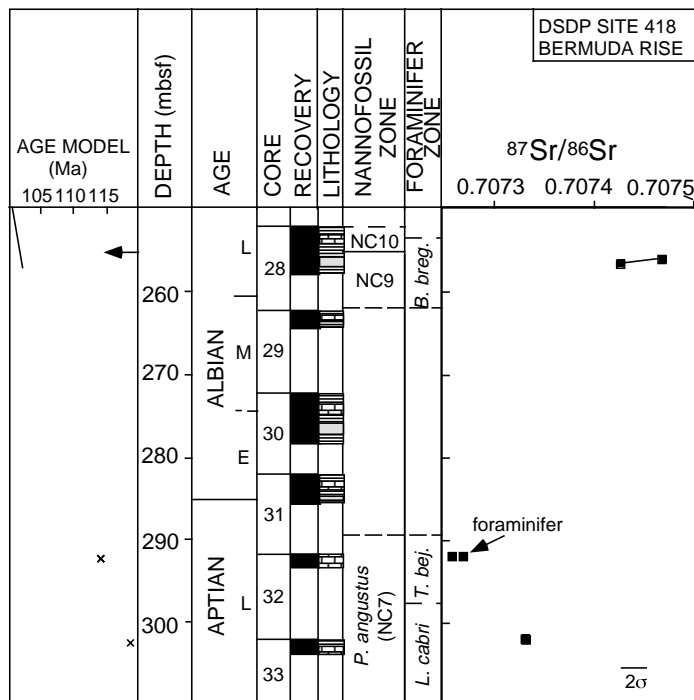

Figure 13. Strontium-isotope analyses of foraminifers from Hole 417D. The nannofossil biostratigraphy is after Gartner (1980) and Siesser (1980). Foraminiferal biostratigraphy is modified after Miles and Orr (1980). An age model is shown on the left; arrows signify tie points (see Table 2). The key to the lithologic column is given in Figure 5; mbsf—meters below sea floor.

Figure 14. Strontium-isotope analyses of foraminifers from Hole 418B. The nannofossil biostratigraphy is after Gartner (1980) and Siesser (1980). Foraminiferal biostratigraphy is modified after Miles and Orr (1980). An age model is shown on the left; the arrow signifies tie point and crosses indicating interpreted ages of samples (see Table 2 and section 2.2). The key to the lithologic column is given in Figure 5; mbsf—meters below sea floor.
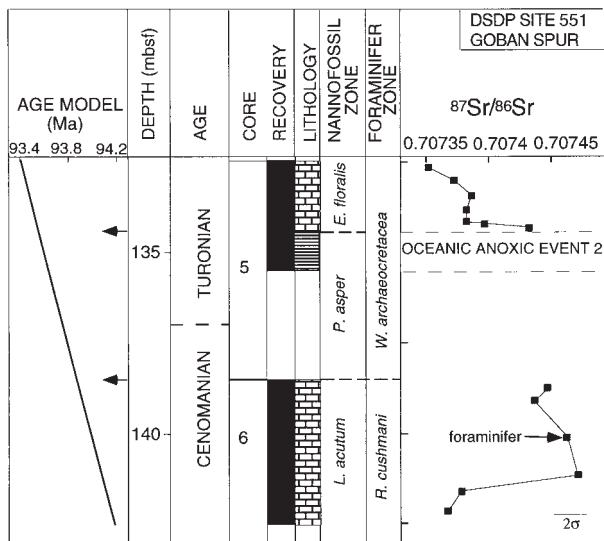
Figure 15. Strontium-isotope analyses of foraminifers from Site 551. The nannofossil biostratigraphy is after Bralower (1988). Planktic foraminiferal biostratigraphy is modified after Graciansky et al. (1985). An age model is shown on the left; arrows signify tie points (see Table 2). Position of oceanic anoxic event (OAE2) of Jenkyns (1980) is shown. The key to the lithologic column is given in Figure 5; mbsf—meters below sea floor.
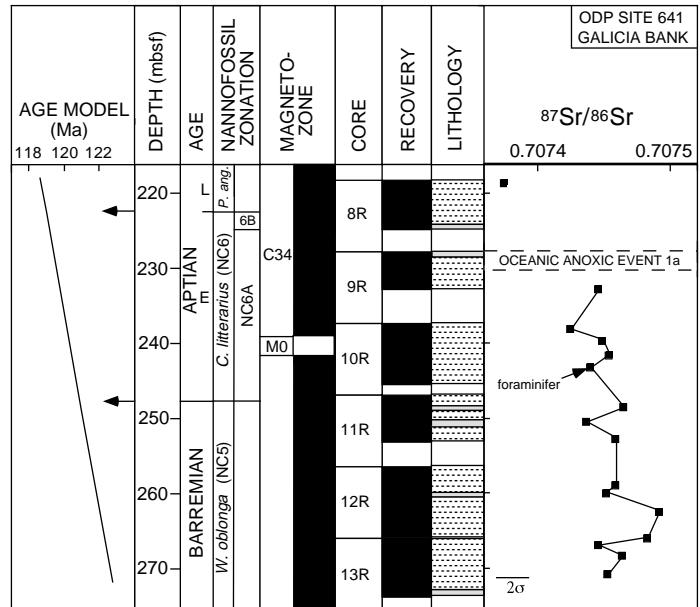
Figure 16. Strontium-isotope analyses of foraminifers from Hole 641C. The nannofossil biostratigraphy is after Applegate and Bergen (1989), modified by Bralower et al. (1994). An age model is shown on the left; arrows signify tie points (see Table 2). Position of oceanic anoxic event OAE1a of Bralower et al. (1993) is shown. The key to the lithologic column is given in Figure 5; mbsf—meters below sea floor.

of clay in a sample can increase the apparent $^{87}Sr/^{86}Sr$ values of carbonates, because some of this Sr could be extracted during the preparation of the sample (e.g., Dasch and Biscaye, 1971; Burke et al., 1982). We have attempted to remove adhering clay from particles prior to analysis, and the dilute (1 M) acetic acid used to dissolve samples minimizes the effect from any remaining clay. In all of the chalk samples analyzed, very little or no clay residue was observed, and such contamination seems unlikely. However, some Sr extraction could have occurred in claystone samples from Sites 545, 547, and 763 where light green clay residues remained in many samples after dissolution.

Trace-Element and Preservational Evidence. SEM observations show some overgrowths of minute rhombs on the inside of chamber walls in almost all foraminiferal samples analyzed, regardless of their pristine appearance (Fig. 4). Volumes of these minute rhombs are negligible compared to the volume of primary calcite in samples from the upper part of Site 511, and Sites 258, 390, 392, 417, and 418. However, in other samples, such as those from the lowermost part of Site 511, and most of those analyzed at Sites 545, 547, and 641, pores and whole chambers are infilled with secondary calcite (Table 3; Fig. 4).

Trace-elemental analyses help identify samples with potentially altered Sr-isotope ratios. Diagenetic calcite tends to have lower Sr/Ca ratios than biogenic calcite (e.g., Baker et al., 1982). Ratios of Na/Ca show the same pattern, whereas Fe/Ca and Mn/Ca ratios in diagenetic calcite may be elevated compared to marine biogenic calcite (e.g., Veizer, 1983). Interpretation of trace-elemental analyses of foraminifers is difficult, however, because a contribution of these elements may be derived from noncalcitic phases coating the outside of tests and filling chambers. Certain phases, such as pyrite and Fe-Mn oxides, may contribute no Sr; others, such as clays and zeolites, may have high Sr contents, at least part of which may be leached by dilute acids during sample preparation. Because of these problems, we use trace-elemental analysis to identify diagenetically altered $^{87}Sr/^{86}Sr$ values in a site-by-site basis.

Ratios of Sr/Ca, Na/Ca, Fe/Ca, Mn/Ca, and Ba/Ca of all foraminiferal samples analyzed are plotted versus age in Figure 17. These plots show significant differences between sites. We believe that these differences result from (1) contamination with Sr-bearing phases such as clays and zeolites in some sites, and non-Sr bearing phases such as Fe-Mn oxides in others, and (2) differences in the amount of calcite recrystallization.

High Sr/Ca, Na/Ca, and Ba/Ca ratios in most samples analyzed at Site 763 (Fig. 17) are thought to result from the presence of zeolites observed growing inside foraminifer tests (Fig. 4i). Strontium-isotope values substantially higher than those in contemporaneous sections (Fig. 18) probably result from the growth of these zeolites from fluids with higher $^{87}Sr/^{86}Sr$ ratios. We note that some of the Sr-isotope fluctuations at Site 763 appear to parallel those at other sites. For example, increases in $^{87}Sr/^{86}Sr$ values in the lowermost Albian stage (between 112 and 110 Ma) correspond to an increase at Site 511 in this same time interval (Fig. 18). This suggests a systematic addition of high-ratio Sr to each sample.

Most foraminifers from Site 547 are nearly filled with calcite (Fig. 4, j–l), and relatively low Sr/Ca and Na/Ca ratios (Fig. 17) are additional indicators of diagenetic alteration. Trace-elemental analyses can also be used to interpret Sr-isotope records with large amounts of variability such as the Aptian part of the record at Site 545 (Fig. 6). Here there is a significant correlation between fluctuations in $^{87}Sr/^{86}Sr$ values, and Sr/Ca and Na/Ca ratios (Fig. 19). Samples with higher $^{87}Sr/^{86}Sr$ values generally possess lower Sr/Ca and Na/Ca ratios, indicating a larger proportion of secondary calcite. In the interval between 390 and 510 mbsf, therefore,
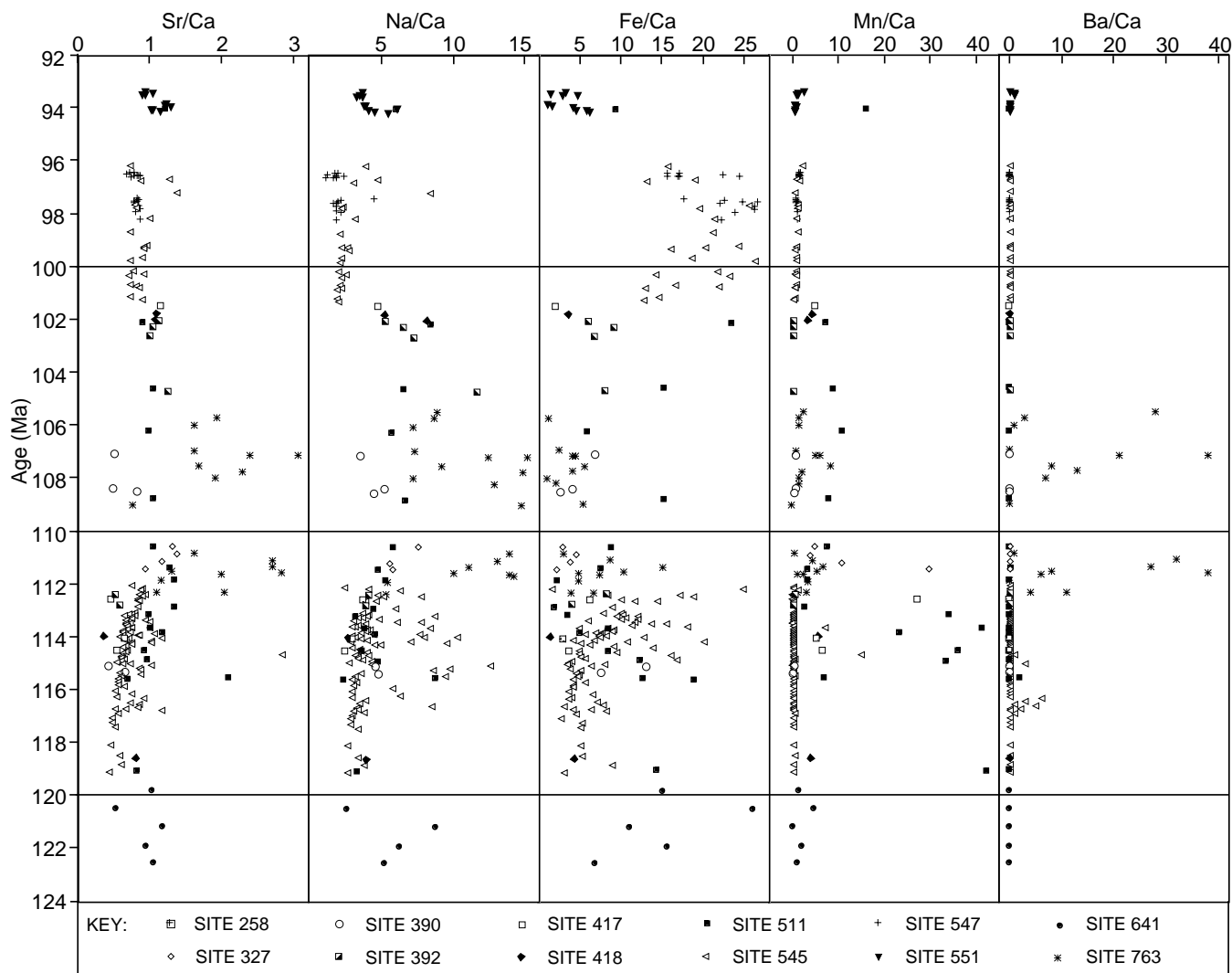
Figure 17. Trace- and minor-element:Ca ratios of foraminifers from all sites investigated plotted vs. the age of samples. A few outlier points have been omitted for each ratio. For data compiled in Table DR1, see footnote 1 in text.

only the samples with the highest Sr/Ca (>0.9) and Na/Ca ratios (>~8) are interpreted as reliable carriers of original Sr-isotope ratios. Strontium-isotope values from the Albian and Cenomanian of Site 545 (390 to 255 mbsf) show much less scatter (Fig. 18) and samples in this interval have generally higher Sr/Ca ratios (Fig. 17). The trace-elemental data suggest a lower degree of recrystallization or a lower clay content, and the Albian and Cenomanian $^{87}Sr/^{86}Sr$ values from Site 545 are thought to be reliable monitors of past seawater.

Comparison of trace-elemental analyses of foraminifers and inoceramids in samples from Site 511 provides an opportunity to evaluate the

effect of diagenesis on $^{87}Sr/^{86}Sr$ values. Above 481 mbsf, where preservation of both groups is excellent, $^{87}Sr/^{86}Sr$ values lie largely within error limits (Fig. 5), suggesting a primary seawater record. Below this depth, infilling of foraminiferal chambers increases and $^{87}Sr/^{86}Sr$ values progressively diverge from those of inoceramids. Alteration of foraminiferal $^{87}Sr/^{86}Sr$ values is indicated by increasing Mn/Ca ratios, generally lower Sr/Ca values (Figs. 17 and 20) and anomalously low $\delta^{18}O$ values (Fassell and Bralower, in press). Because the Site 511 inoce-ramid $^{87}Sr/^{86}Sr$ values show less variability, and are generally slightly lower than those of foraminifers (Figs. 3 and 5), and because inoce-

ramids possess more uniform trace-element contents (Fig. 20), we utilize them in developing the seawater Sr-isotope curve.

Stacking of $^{87}Sr/^{86}Sr$ Values from Different Sites and Construction of the Composite Record. When all of the $^{87}Sr/^{86}Sr$ values of contemporaneous samples from different locations are stacked (Fig. 18), a significant amount of scatter exists. However, when all of the samples with indications of diagenetic alteration or suspect age are removed, a much narrower band at the lower limits of the total range is defined (Fig. 21). We maintain that this band represents the best record of seawater Sr-isotope variation and use the $^{87}Sr/^{86}Sr$ values in this common band
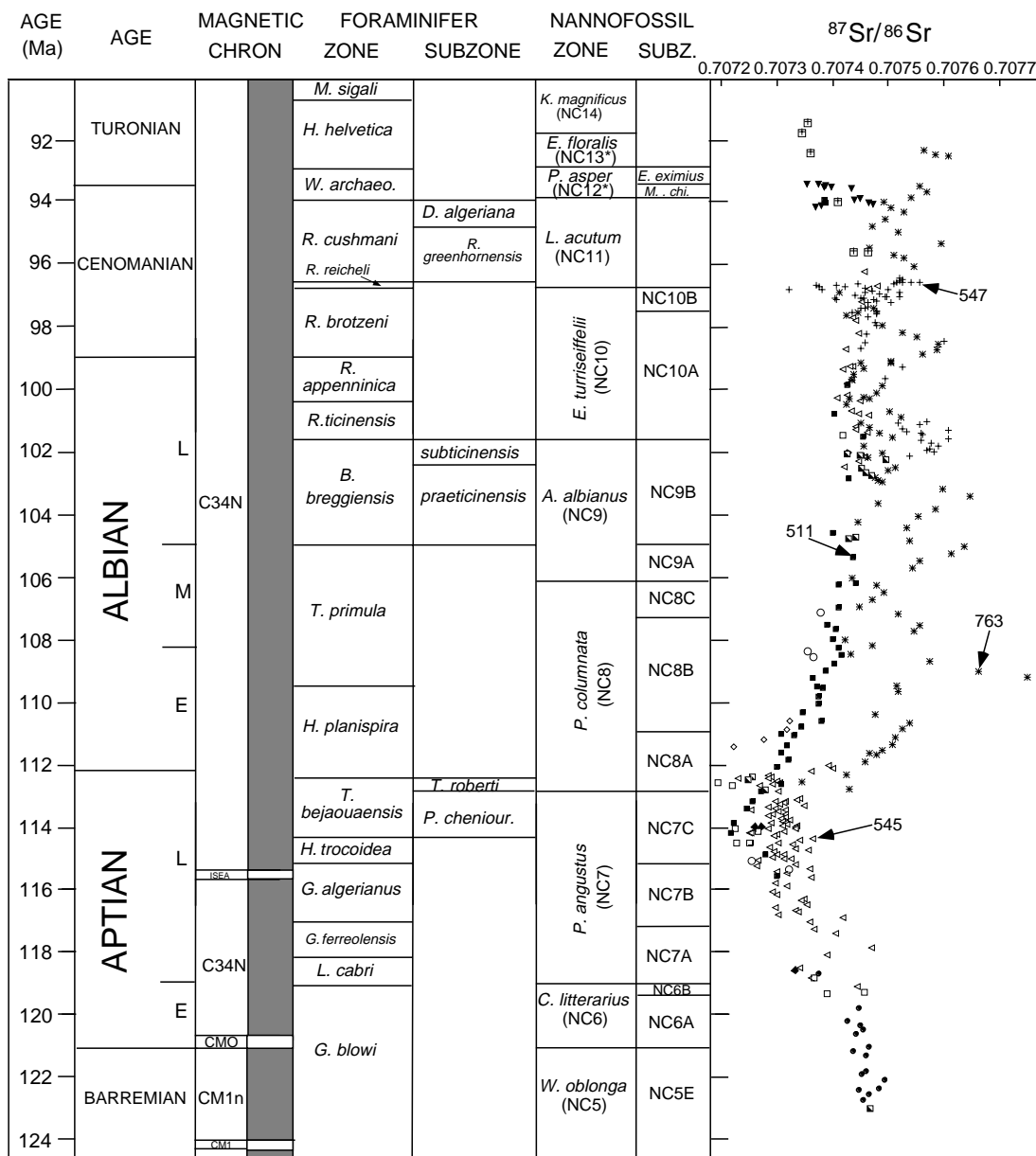
Figure 18. The strontium-isotope data from all sites investigated. Disparities between nannofossil and planktic foraminiferal biostratigraphies of individual sections lead to minor inconsistencies in ages plotted vs. the integrated chronology (Fig. 2). The key to the symbols is given in Figure 17.

to define our composite record. The 150 data points used in the composite record include: (1) all measurements of foraminifers from Sites 258, 390, 417, 418, 551, and 641, (2) all inoceramid analyses from Sites 327, 392, and 511 (and foraminiferal measurements in the former two sites in samples in which no inoceramid analyses were performed), and (3) Cenomanian, Albian, and certain Aptian data points from Site 545 (see above discussion). Strontium-isotope values of some 230 samples, including many from Site

545, and most from Sites 547 and 763 lie significantly above this band (Fig. 18). We maintain that the ^{87}Sr/^{86}Sr values of these samples have increased during diagenesis.

Deep-Sea Sr-Isotope Stratigraphy

The composite record shows a decrease in ^{87}Sr/^{86}Sr values from just over 0.70745 in the late Barremian stage to just over 0.70720 in the late Aptian stage (Fig. 21). Strontium-isotope

values begin to increase close to the Aptian-Albian boundary, rise rapidly in the early Albian and remain close to 0.70745 from the middle Albian to the late Cenomanian stages. A sharp decrease in ^{87}Sr/^{86}Sr values occurs just above the Cenomanian-Turonian boundary; earliest Turonian values average 0.70735. The curve produced by local linear smoothing (hereafter referred to as the smoothed composite curve) accounts for most of the variation shown by the composite data set (Fig. 22A). One exception is in the latest
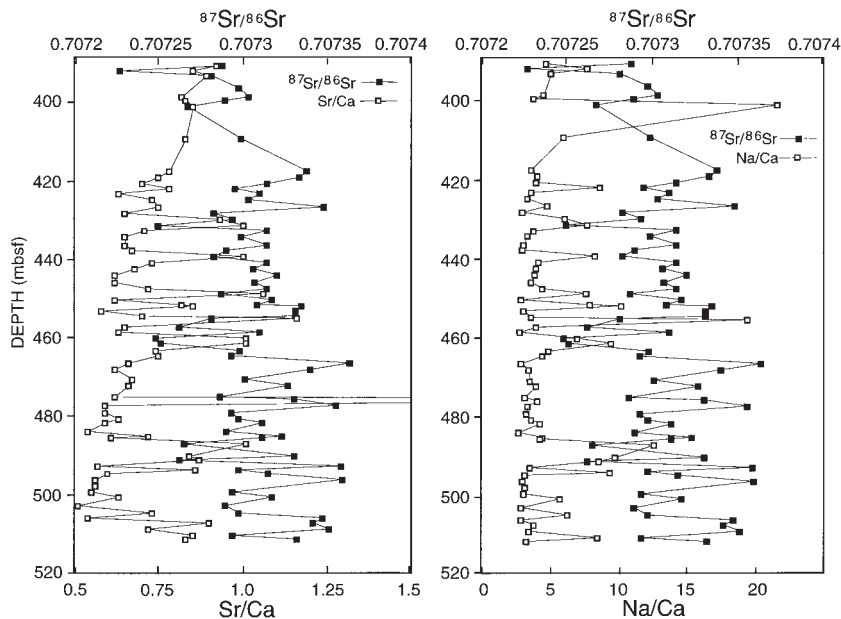
Figure 19. Sr/Ca and Na/Ca ratios (µmol/mol) plotted vs. $^{87}Sr/^{86}Sr$ values of samples in the Aptian section of Site 545. Pearson correlation coefficients for $^{87}Sr/^{86}Sr$ values vs. Sr/Ca and Na/Ca are –0.53 and –0.43, respectively which are both significant at the 99% interval of confidence. See text for discussion.

Aptian (*Ticinella bejaouaensis* foraminiferal zone), where a short-term increase in $^{87}Sr/^{86}Sr$ values is seen in Sites 392, 418, and 545, but not in Sites 417 and 511. Although we believe that the lower $^{87}Sr/^{86}Sr$ values are more reliable, and thus the trough in the late Aptian stage may actually be slightly larger than the smoothed composite curve indicates, the possibility of two smaller troughs with a minor saddle in the *T. bejaouaensis* zone cannot be dismissed.

Comparison of our composite deep-sea Sr-isotope record with published data sets shows both similarities and differences. The smoothed composite curve shows a close resemblance to the values of McArthur et al. (1994) for the Cenomanian–early Turonian (Fig. 22E). The composite data show significantly less scatter than those of Ingram et al. (1994) (Fig. 22, A and B). We have smoothed the Sr-isotope ratios of Ingram et al. (1994), including both original and revised (Tarduno et al., 1989) biostratigraphic ages of the samples of Koepnick et al. (1985) from Site 167, and make the following observations: (1) smooths from the corrected and uncorrected data are approximately parallel to the smoothed composite curve, but $^{87}Sr/^{86}Sr$ values of Ingram et al. (1994) are higher by an average of 0.0001–0.00015 (Fig. 22B); (2) smoothed curves drawn through the Ingram et al. (1994) data set show a considerably smaller

Aptian-Albian trough than the curve drawn by Ingram et al. (1994); and (3) if two age points at 111.4 and 112.6 Ma are excluded, the trough in the smoothed curve of the Ingram et al. (1994) data set virtually disappears. Thus we conclude that the curve of Ingram et al. (1994) is arbitrarily drawn. We postulate that the differences between the Ingram et al. (1994) data set and the composite result from addition of Sr with relatively high $^{87}Sr/^{86}Sr$ values during diagenesis, and/or from the difficulty of removing particles such as clay with high $^{87}Sr/^{86}Sr$ values from the fish teeth.

The shape of our composite curve is comparable to that defined by the Barremian-Albian data of Jones et al. (1994b); however, it is clear that there are consistent age offsets of as much as 4 m.y. (Fig. 22C). The analyses of Jones et al. (1994b) derive from well-preserved clam and oysters in shallow-water sections from England. Ages in these sections were determined using Boreal ammonite-subzonal and stage-boundary definitions assuming equal subzone durations. We have used existing nannofossil zonal-ammonite subzonal correlations (Table 4) to recalibrate the Jones et al. (1994b) data set and produce a modified curve by smoothing. The resulting curve lies remarkably close to the smoothed composite curve (Fig. 22D). The apparently larger scatter of the composite compared

to the Jones et al. (1994b) and McArthur et al. (1994) data sets is likely a result of (1) the significantly larger size of our data set, and (2) the longer durations of the microfossil zonal units than ammonite subzones.

The composite Sr-isotope record shows remarkable similarity to the curve of Jenkyns et al. (1995) obtained from the analysis of shallow-water limestones recovered in ODP Site 866 from Resolution Guyot in the central Pacific (Fig. 22F). This independent data set provides additional support for the composite Sr-isotope record.

The steeper portions of the smoothed composite curve offer significant chronologic potential, especially for unfossiliferous sedimentary rocks. We offer polynomial and linear equations fitting three portions of the smoothed composite curve (Table 5).

Our data allow correlation of Sr-isotope values with microfossil zonal boundaries, and thus modification of previous correlations of the Sr-isotope stratigraphy and stage boundaries. Two boundaries lie at diagnostic points in the composite curve: the Aptian-Albian boundary is close to the minimum $^{87}Sr/^{86}Sr$ value in the broad Aptian–early Albian $^{87}Sr/^{86}Sr$ trough, and $^{87}Sr/^{86}Sr$ values decrease rapidly just above the Cenomanian-Turonian boundary (Figs. 21 and 22A). Therefore the composite Sr-isotope stratigraphy has potential for helping to identify these stage boundaries.

Geologic Significance of Mid-Cretaceous Sr-Isotope Curves

Case for High Crustal Production Rates. Larson (1991) and Larson and Olson (1991) proposed that the volume of mid-plate volcanic plateaus formed in the mid-Cretaceous was almost three times greater and that production of ridge-crest crust was 28% higher than in prior and subsequent time intervals. Coincidence of high mid-plate and ridge-crest crustal production rates is thought to have resulted from a mantle plume that fueled volcanism in both settings (e.g., Larson and Kincaid, 1996).

Isotopic, biostratigraphic, and magnetostratigraphic age constraints of mid-Cretaceous mid-plate and ridge-crest crust are few, however. For example, a major episode of flood basalt volcanism occurred in the late Barremian to early Aptian stages when the Hess Rise and the Ontong Java and Manihiki Plateaus in the central and western Pacific were constructed (Schlanger et al., 1981; Duncan and Richards, 1990; Tarduno et al., 1991). The age of the largest and best dated of these features, the Ontong Java Plateau, is constrained by isotopic dates on basalts from only four locations. These dates range between 120 and 124 Ma, but cluster between 121.5 and
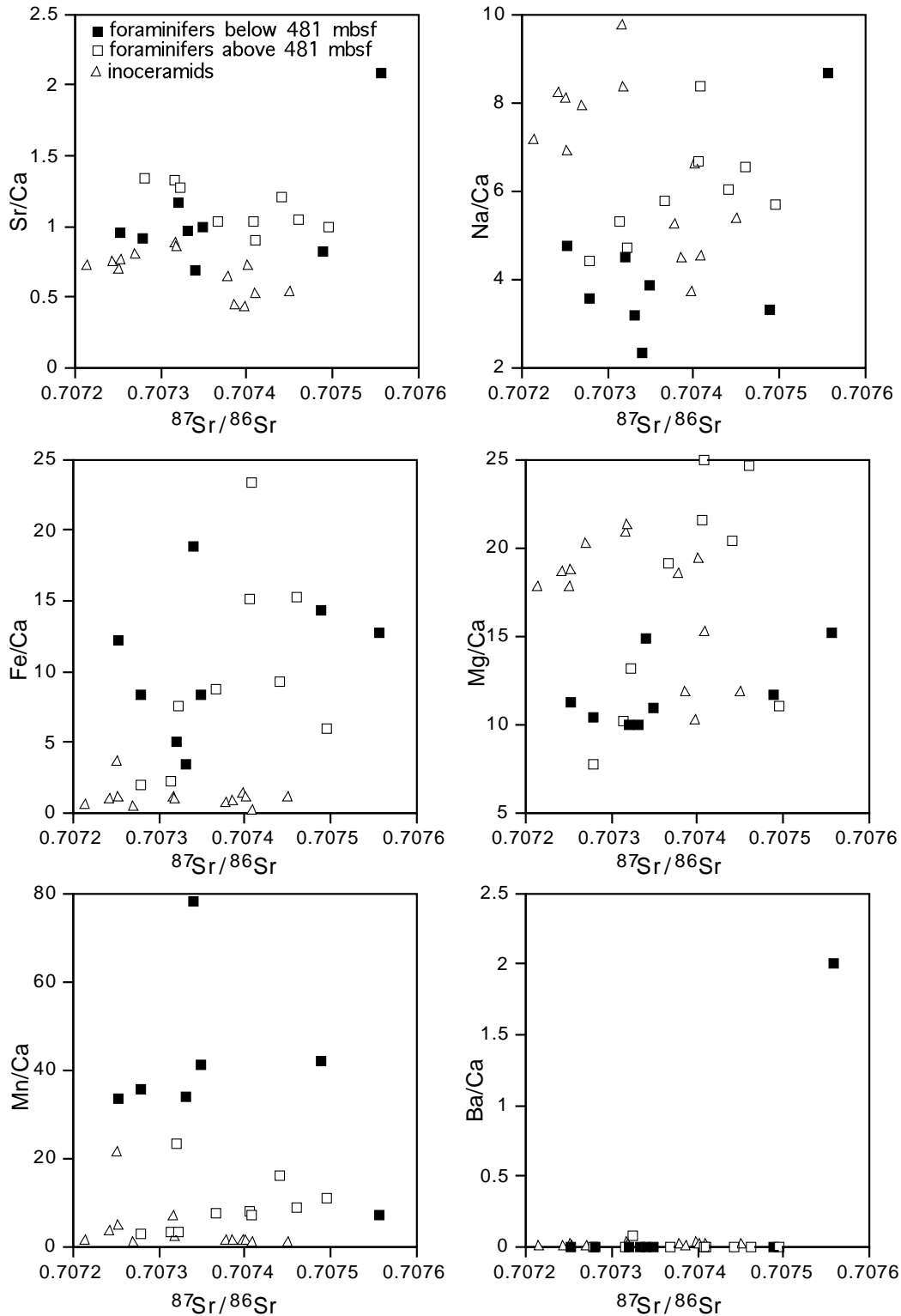
Figure 20. Elemental ratios (µmol/mol) plotted vs. $^{87}Sr/^{86}Sr$ values of samples from Site 511. Open squares refer to foraminiferal analyses from above 481 m below the sea floor (mbsf) (section 511-55-1 and up); closed squares refer to foraminiferal analyses from below 481 mbsf (section 511-55-2 and down); triangles refer to inoceramid analyses.
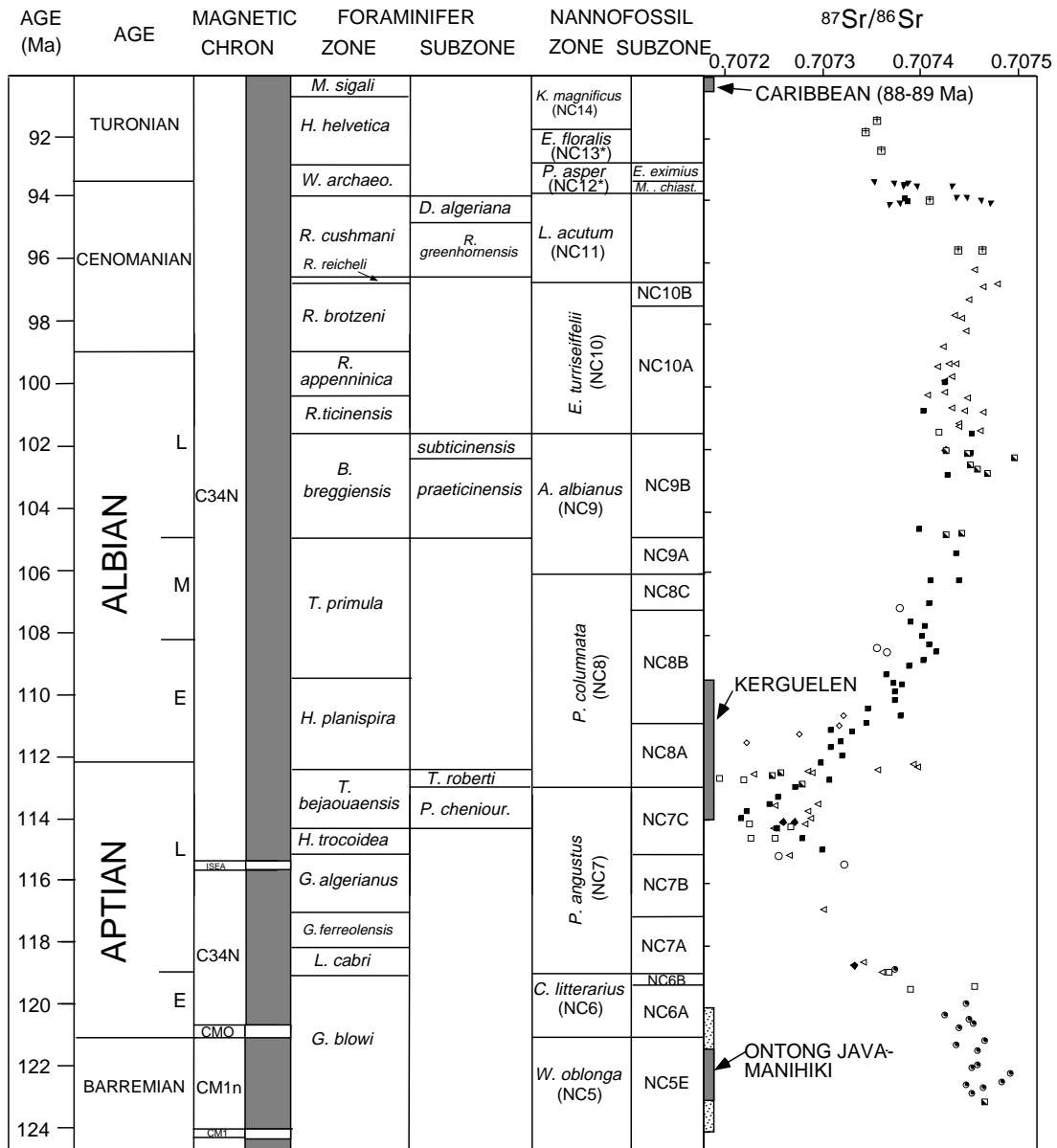
Figure 21. Composite Sr-isotope data set. All samples are plotted except those from Sites 547, 763, and selected samples from Site 545 (see text for discussion). Disparities between nannofossil and planktic foraminiferal bio-stratigraphies of individual sections lead to minor inconsistencies in ages plotted against the integrated chronology (Fig. 2). Isotopic ages of mid-plate volcanic episodes are shown (dark shaded pattern refers to cluster of ages of Ontong Java and Manihiki plateaus; light shaded pattern refers to total range of ages). The key to the symbols is given in Figure 17.
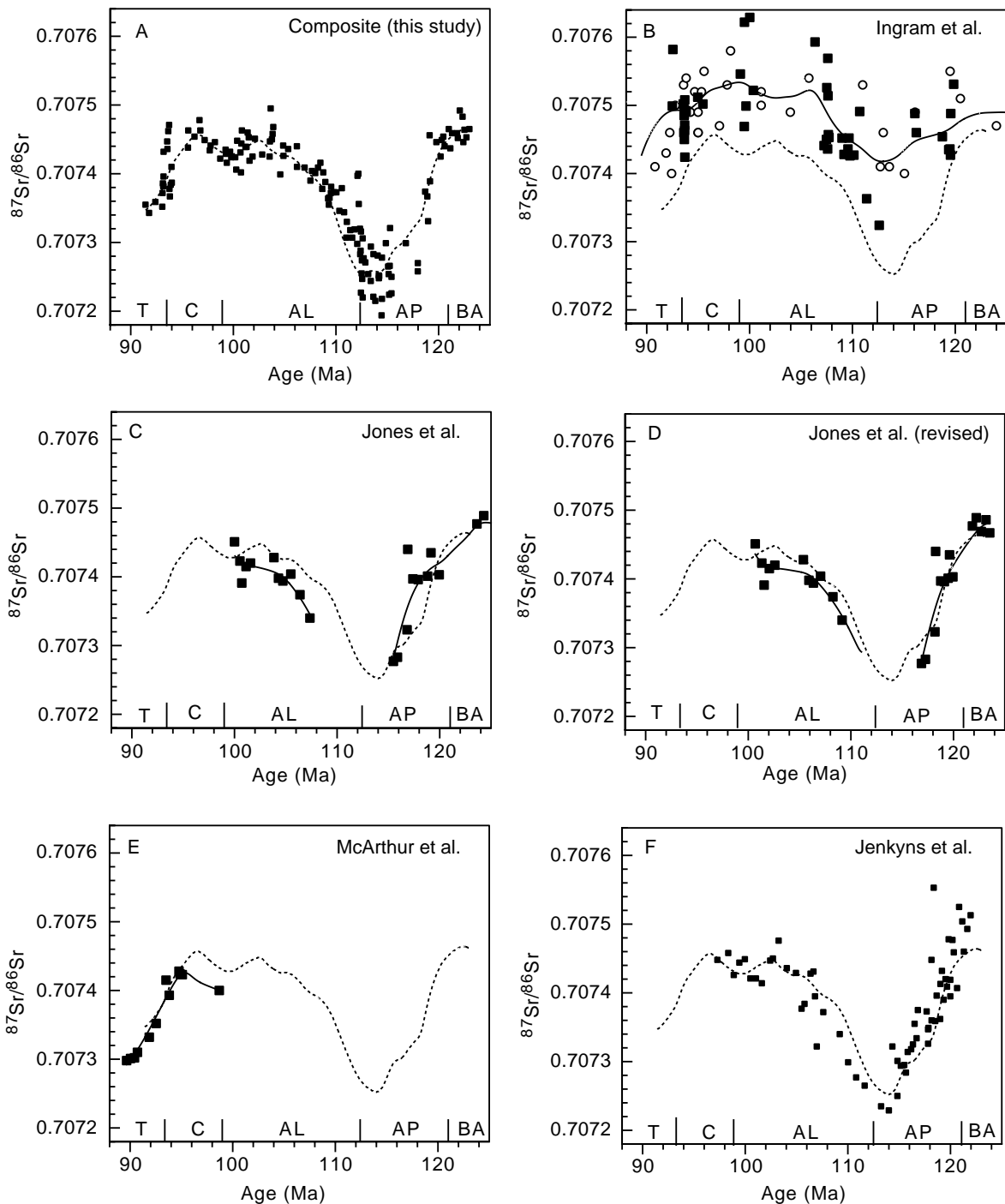
Figure 22. Comparison of (A) composite data set (this study) with data sets of (B) Ingram et al. (1994). Squares are data points of samples analyzed by Ingram et al. (1994); circles are points taken from Koepnick et al. (1985) with revised biostratigraphy from Tarduno et al. (1989). Note that biostratigraphic corrections result in age errors of as much as 10 m.y.; both Ingram et al. (1994) and Koepnick et al. (1985) data sets are calibrated to Gradstein et al. (1994) time scale. (C, D) Jones et al. (1994b), (E) McArthur et al. (1994), and (F) Jenkyns et al. (1995). Solid curve in each graph (except F) shows the local-linear smooth of the data set (see Fan and Gijbels [1996] for a description of this technique); dashed curve shows the smoothed composite curve. The kernel function used for the local-linear smooth is the Gaussian function with a bandwidth of 0.75 for the data collected here, and 1.5 for the data sets of other authors. The higher bandwidth is a result of the lower sample density of previous studies. Because of the data gap in C and D, the data sets are divided in two at the gap, and two shorter curves are generated. The ages of samples in F were calculated using tie points from the composite curve (A) as follows: 97 Ma—0 m below sea floor (mbsf), 104 Ma—250 mbsf, 107 Ma—350 mbsf, 114 Ma—434.5 mbsf, 122 Ma—900 mbsf, and assuming constant sedimentation rates in between. On the basis of analyses on NBS-SRM987, we have added 0.00011 to the $^{87}Sr/^{86}Sr$ analyses of Koepnick et al. (1985) and 0.000025 to the values of Jones et al. (1994b), and subtracted 0.000025 from the values of Ingram et al. (1994). Positions of stage boundaries are shown.

TABLE 4. CORRELATION OF BOREAL AMMONITE SUBZONES AND NANNOFOSSIL ZONES

Nanno zone	Ammonite subzone	References
Base NC10	**Between *Callihoplites auritus* and *Diploceras cristatum***	Thierstein (1973); Taylor (1982)
	Mortoniceras rostratum*	Jeremiah (1996)
Base NC9	Between *Euhoplites nitidus* and *Dimorphoplites niobe*	Thierstein (1973)
	Euhoplites nitidus	Taylor (1982)
	Between *Anahoplites intermedius* and *D. niobe*†	Crux (1991)
	Hoplites spathi	Jeremiah (1996)
Base NC8	Between *Dimorphosus niobe* and *Anahoplites intermedius*	Thierstein (1973)
	Lyelliceras lyelli	Afejuku (1980), Taylor (1982)
	Middle of the *Leymeriella tardefurcata* zone§	Mutterlose (1992), Keupp and Mutterlose (1994)
	Othoplites bulliensis	Jeremiah (1996)
Base NC7	*Cheloniceras debile*	Taylor (1982)
	***Deshayesites grandis* #**	Mutterlose (1992), Keupp and Mutterlose (1994)
Base NC6	**Between *Parancyloceras bidentatum* and *Prodeshayesites fissicostatus* zones**	Mutterlose (1992), Keupp and Mutterlose (1994)

Note: Accepted correlations shown in bold type.
*Would result in unrealistically high sedimentation rates for the upper part of the Gault Clay.
†Study more detailed.
§All other schemes result in unrealistically high sedimentation rates for the lower part of the Gault Clay.
#Investigations based on outcrops as well as cored boreholes.

TABLE 5. EQUATIONS FOR PORTIONS OF THE COMPOSITE CURVE

(1) 114–119.5 Ma $\text{Age} = -179168021.14 \, (^{87}Sr/^{86}Sr)^2 + 253497831.92 \, (^{87}Sr/^{86}Sr) - 89665924.65$
(2) 106–112 Ma $\text{Age} = -249985102.78 \, (^{87}Sr/^{86}Sr)^2 + 353614151.81 \, (^{87}Sr/^{86}Sr) - 125050308.29$
(3) 91.5–95 Ma $\text{Age} = 36505.89 \, (^{87}Sr/^{86}Sr) - 25730.56$

123 Ma (weighted mean = 122.4 ± 0.8 Ma) (Mahoney et al., 1993; Tejada et al., 1996). Paleomagnetic data show that interbedded limestone and basalt at Ontong Java Plateau Site 807 are normally magnetized and are thought to correlate to the Cretaceous long-normal polarity interval (Tarduno et al., 1991). Combined with biostratigraphic data (Erba, 1994), this suggests an early Aptian age (between about 120.5 and 120 Ma in the Gradstein et al. [1994] time scale). The inconsistency between the biostratigraphic and isotopic ages from Ontong Java may suggest that the age of M0 in the Gradstein et al. (1994) time scale is slightly too young, or that the duration of Ontong Java volcanism was longer than previous estimates (Tarduno et al., 1991). Although it is impossible to differentiate between these alternatives, we assume the full range of Ontong Java ages from biostratigraphic, paleomagnetic, and isotopic data (Fig. 21).

The Manihiki Plateau is isotopically dated in only one location (123 Ma; Mahoney et al., 1993). The large Kerguelen Plateau in the southern Indian Ocean apparently formed in a relatively short period of time, between 114 and 110 Ma (Whitechurch et al., 1992; Coffin and Eldholm, 1994), but this inference is based on isotopic ages from only four locations. Rates of ridge-crest crustal production (e.g., Kominz, 1984) are complicated by the Cretaceous long-normal polarity interval, which makes it difficult to assess relative changes in crustal production over the 38 m.y. duration of the chron, and to de-

tect ridge jumps and plate reorganizations that, if unrecognized, artificially inflate estimates of crustal production (Heller et al., 1996). The Cretaceous long normal in the Gradstein et al. (1994) time scale begins at 120.5 Ma and ends at 83.5 Ma (Gradstein et al, 1994). This implies a shorter duration than that assumed by Larson (1991), and thus would increase somewhat the magnitude of ocean-ridge crustal production.

Significance of Sr Isotopes to Crustal Production Estimates. The Aptian-Albian decrease in seawater $^{87}Sr/^{86}Sr$ values is compatible with increased rates of hydrothermal activity associated with increased rates of ocean-crust production (Jones et al., 1994b; Ingram et al., 1994). However, the oceanic ridges (Jones et al., 1994b; Larson, 1994) and plateaus (Ingram et al., 1994; Ingram and Richter, 1994) have both been identified as sources of increased hydrothermal Sr.

The composite seawater Sr-isotope curve offers evidence for the timing of the potentially enhanced mid-Cretaceous ocean crust production, as well as a sense of the relative magnitude of crustal production through time. The onset of accelerated crust production is well dated by the records derived from Sites 417 and 641. In both cases, the decrease in $^{87}Sr/^{86}Sr$ values starts several meters above M0 (Figs. 13 and 16). If a large plume is responsible for both the long-normal polarity interval and accelerated ocean-ridge crustal production (Larson and Olson, 1991), then the 0.5 to 1 m.y. lag between the beginning of the long-normal and the onset of the

decrease in seawater $^{87}Sr/^{86}Sr$ values may reflect the long (several million years) residence time of Sr as well as the time required for Sr to be leached from the new crust. If mid-plate hydrothermal activity were the sole source of volcanic Sr (Ingram et al., 1994), and most of the volcanism on the Ontong Java and Manihiki Plateaus had terminated by 120 Ma, as available data suggest (e.g., Tarduno et al., 1991; Mahoney et al., 1993), then the seawater Sr isotope decrease also lags slightly the end of the volcanic pulse (Fig. 21).

Ingram et al. (1994) interpreted their Aptian-Albian Sr-isotope data in terms of two negative excursions, each associated with the eruption of a large igneous province (Ontong Java and Kerguelen Plateaus). However, local-linear smoothing of all of the relevant data sets shows a single decrease in $^{87}Sr/^{86}Sr$ values in the Aptian-Albian stages (Fig. 22, A, C and F), not two as would be expected if the current dates for the Ontong Java, Manihiki, and Kerguelen Plateaus are representative. If volcanism ceased in most locations on Ontong Java by 121.5 Ma (Mahoney et al., 1993) and on Manihiki at 123 Ma, there is a 6 m.y. gap between volcanism on these plateaus and Kerguelen at a time when Sr-isotope ratios in the composite curve are descending rapidly (Fig. 21).

The timing of the onset of the early Aptian decrease in $^{87}Sr/^{86}Sr$ values combined with the shape of the composite Sr-curve suggest that either the current isotopic ages for the oceanic plateaus are not representative, or that leaching

of Sr from oceanic plateaus takes millions of years, or that another source, the ridge crests or a subducted plateau, supplied volcanic Sr to the oceans. Without more isotopic ages from mid-plate features, it is difficult to conclusively differentiate between these alternatives. However, the existing ages interpreted in light of the composite Sr-isotope curve support the notion of increased oceanic-ridge crustal production during the Aptian–early Albian stages.

Ingram et al. (1994) correlated the decrease in $^{87}Sr/^{86}Sr$ values around the Cenomanian-Turonian boundary (93.5 Ma in Gradstein et al. [1994]) with mid-plate volcanism that produced the Caribbean plate. However, available isotopic dates from the Caribbean range between 88 and 89 Ma (e.g., Duncan et al., 1994) (Fig. 21). Low $^{87}Sr/^{86}Sr$ values extend from the early Turonian through the Coniacian (McArthur et al., 1994), and part of this interval corresponds to the Caribbean volcanism and secondary volcanic phases on the Kerguelen and Ontong Java Plateaus between 89 and 85 Ma (Duncan et al., 1994; Bercovici and Mahoney, 1994).

The composite curve suggests that a 15 m.y. interval encompassing the middle Albian–late Cenomanian was not associated with increased volcanic Sr flux. These data conflict with Larson's (1991) crustal production curve, which suggests that there was increased crustal production over this interval. Unfortunately, the Sr-isotope record is limited in that it cannot yet place constraints on the absolute magnitude of enhanced crustal production in the mid-Cretaceous. In addition to uncertainties in the relative contributions of mid-plate and ocean-ridge hydrothermal activity, the relationship between increased crustal production and increased hydrothermal Sr flux is not well established, and the response of weathering rates to any increased CO_2 fluxes to the atmosphere is not well understood (Kump, 1989; Berner, 1990; Caldeira and Rampino, 1991; Jones et al., 1994b).

Seawater Sr-Isotope Curves: Volcanism and Anoxic Events. Several authors have commented on possible relationships between "anoxic events," volcanism, and the Sr-isotope record (e.g., Vogt, 1989; Jones and Jenkyns, 1995). The coincidence in timing between lowered $^{87}Sr/^{86}Sr$ values and deposition of organic-rich sediments is thought to be indirectly linked through sea level and volcanism. The close synchroneity of the onset of early Aptian volcanic activity and the "Selli" anoxic event (OAE1a) (e.g., Coccioni et al., 1987) can be seen in Sr-isotope data from Site 641. Here, the onset of the decrease in $^{87}Sr/^{86}Sr$ values leading to the Aptian trough correlates closely with an interval lacking calcareous microfossils which corresponds to the anoxic event (Bralower et al., 1994) (Fig. 16).

Strontium-isotope values from Site 551 increase just below the organic-rich sediments deposited during the Cenomanian-Turonian boundary oceanic anoxic event (Bralower, 1988), but show a substantial decrease immediately above (Fig. 15). Although we have no explanation for the increase in $^{87}Sr/^{86}Sr$ values below the black shale, we tentatively conclude that the decrease in $^{87}Sr/^{86}Sr$ values probably resulted from a volcanic episode that led to the major early Turonian transgression (e.g., Haq et al., 1987).

SUMMARY

An investigation of mid-Cretaceous seawater Sr-isotope stratigraphy was carried out by measuring foraminifers and inoceramid bivalves from 12 DSDP and ODP sections. Diagenetic alteration is identified by observing fossil preservation, measuring trace elements, and stacking $^{87}Sr/^{86}Sr$ values of samples of similar age. The composite curve formed by samples that have undergone little or no alteration shows a trough of low $^{87}Sr/^{86}Sr$ values in the Aptian and early Albian stages, higher but constant values for the rest of the Albian and Cenomanian stages, followed by a decrease in $^{87}Sr/^{86}Sr$ values in the early Turonian stage. Disparities between the composite curve and published Sr-isotope stratigraphies are largely related to the different biostratigraphies and assumptions used to estimate age, rather than to diagenesis and analytical procedures. The age and shape of the trough in $^{87}Sr/^{86}Sr$ values in the Aptian-Albian stages combined with the available isotopic age dates are consistent with some volcanic Sr being derived from increased crustal production rates at spreading centers.

ACKNOWLEDGMENTS

REFERENCES CITED

Afejuku, A., 1980, Albian to Cenomanian calcareous nannoplankton from N.W. Europe [Ph.D. thesis]: London, University of London, 247 p.

Applegate, J. L., and Bergen, J. A., 1988, Cretaceous calcareous nannofossil biostratigraphy of sediments recovered from the Galicia Margin, ODP Leg 103, in Boillot, G., Winterer, E. L., et al., eds., Proceedings of the Ocean Drilling Program, Scientific results, Volume 103: College Station, Texas, Ocean Drilling Program, p. 293–319.

Baker, P. A., Gieskes, J. M., and Elderfield, H., 1982, Diagenesis of carbonates in deep-sea sediments: Evidence from Ca/Sr ratios and interstitial dissolved Sr^{2+} data: Journal of Sedimentary Petrology, v. 52, p. 71–82.

Barron, E. J., Harrison, C. G., Sloan, J. L., II, and Hay, W. W., 1981, Paleogeography, 180 million years ago to the present: Eclogae Geologicae Helvetiae, v. 74, p. 443–470.

Bercovici, D., and Mahoney, J., 1994, Double flood basalts and plume head separation at the 660-kilometer discontinuity: Science, v. 266, p. 1367–1369.

Berger, W. H., 1974, Deep-sea sedimentation, in Burk, C. A., and Drake, C. D., eds., The geology of continental margins: New York, Springer-Verlag, p. 213–241.

Berner, R. A., 1990, Atmospheric carbon dioxide over Phanerozoic time: Science, v. 249, p. 1382–1386.

Bralower, T. J., 1988, Calcareous nannofossil biostratigraphy and assemblages of the Cenomanian-Turonian boundary interval: Implications for the origin and timing of oceanic anoxia: Paleoceanography, v. 3, p. 275–316.

Bralower, T. J., 1992, Aptian-Albian calcareous nannofossil biostratigraphy of ODP Site 763 and the correlation between high- and low-latitude zonations, in Duncan, R. A., Rea, D. K., Kidd, R. B., von Rad, U., and Weissel, J. K., eds., Synthesis of results from drilling in the Indian Ocean: American Geophysical Union Monograph 70, p. 245–252.

Bralower, T. J., and Siesser, W. G., 1992, Cretaceous calcareous nannofossil stratigraphy of ODP Sites 761, 762 and 763, Exmouth and Wombat Plateaus, N.W. Australia, in von Rad, U., Haq, B. U., et al., eds., Proceedings of the Ocean Drilling Program, Scientific results, Volume 122: College Station, Texas, Ocean Drilling Program, p. 529–566.

Bralower, T. J., Sliter, W. V., Arthur, M. A., Leckie, R. M., Allard, D. J., and Schlanger, S. O., 1993, Dysoxic/anoxic episodes in the Aptian-Albian, in Pringle, M. S., Sager, W. W., Sliter, W. V., and Stein, S., eds., The Mesozoic Pacific: Geology, tectonics, and volcanism: American Geophysical Union Monograph 77, p. 5–37.

Bralower, T. J., Arthur, M. A., Leckie, R. M., Sliter, W. V., Allard, D. J., and Schlanger, S. O., 1994, Timing and paleoceanography of oceanic dysoxia/anoxia in the late Barremian to early Aptian (Early Cretaceous): Palaios, v. 9, p. 335–369.

Brass, G. W., 1976, The variation of the marine $^{87}Sr/^{86}Sr$ ratio during the Phanerozoic time: Interpretation using a flux model: Geochimica et Cosmochimica Acta, v. 40, p. 721–730.

Burke, W. H., Denison, R. E., Hetherington, E. A., Koepnick, R. B., Nelson, H. F., and Otto, J. B., 1982, Variation of seawater $^{87}Sr/^{86}Sr$ throughout Phanerozoic time: Geology, v. 10, p. 516–519.

Caldeira, K., and Rampino, M. R., 1991, The mid-Cretaceous super-plume, carbon dioxide, and global warming: Geophysical Research Letters, v. 18, p. 987–990.

Coccioni, R., Nesci, O., Tramontana, M., Wezel, F. -C., and Moretti, E., 1987, Descrizione di un livello-guida "Radiolaritic-bituminoso-ittiolitico" alla base delle Marne a Fucoidi nell'Appennino Umbro-Marchigiano: Bolletino della Società Geologica Italiana, v. 106, p. 183–192.

Coffin, M. F., and Eldholm, O., 1994, Large igneous provinces: Crustal structure, dimensions, and external consequences: Reviews of Geophysics, v. 32, p. 1–36.

Crux, J. A., 1991. Albian calcareous nannofossils from the Gault Clay of Munday's Hill (Bedfordshire, England): Journal of Micropalaeontology, v. 10, p. 203–222.

Dasch, E. J., and Biscaye, P. E., 1971, Isotopic composition of strontium in Cretaceous to Holocene pelagic foraminifera: Earth and Planetary Science Letters, v. 11, p. 201–204.

Denison, R. E., Koepnick, R. B., Fletcher, A., Dahl, D. A., and Baker, M. C., 1993, Reevaluation of early Oligocene,

Eocene, and Paleocene seawater strontium isotope ratios using outcrop samples from the U.S. Gulf Coast: Paleoceanography, v. 8, p. 101–126.

DePaolo, D. J., and Finger, K. L., 1991, High resolution strontium isotope stratigraphy and biostratigraphy of the Miocene Monterey Formation, central California: Geological Society of America Bulletin, v. 103, p. 112–124.

DePaolo, D. J., and Ingram, B. L., 1985, High resolution stratigraphy with strontium isotopes: Science, v. 227, p. 938–941.

Duncan R. A., and Richards, M. A., 1990, Early Cretaceous global flood basalt volcanism: Eos (Transactions, American Geophysical Union), v. 71, p. 1668.

Duncan, R. A., Sinton, C. W., and Donnelly, T. W., 1994, The Caribbean Cretaceous basalt province: An oceanic LIP: Eos (Transactions, American Geophysical Union), v. 75, p. 594.

Elderfield, H., and Gieskes, J. M., 1982, Sr isotopes in interstitial waters of marine sediments from Deep-Sea Drilling Project cores: Nature, v. 300, p. 493–497.

Erba, E., Premoli Silva, I., and Watkins, D. K., 1996, Cretaceous calcareous plankton biostratigraphy of Sites 872 through 879, in Haggerty, J. A., Premoli Silva, I., Rack, F., and McNutt, M. K., eds., Proceedings of the Ocean Drilling Program, Scientific results, Volume 144: College Station, Texas, Ocean Drilling Program, p. 157–169.

Fan, J., and Gijbels, I., 1996, Local polynomial modeling and its applications: London, Chapman and Hall, 341 p.

Farrell, J. W., Clemens, S. C., and Gromet, L. P., 1995, Improved chronostratigraphic reference curve of late Neogene seawater $^{87}Sr/^{86}Sr$: Geology, v. 23, p. 403–406.

Fassell, M. L., and Bralower, T. J., in press, A warm, equable mid-Cretaceous: Stable isotope evidence, in Barrera, E., and Johnson, C., eds., The evolution of Cretaceous ocean/climate systems: Geological Society of America Special Paper.

Gartner, S., Jr., 1980, Calcareous nannofossils, Deep Sea Drilling Project Holes 418A and 418B, in Donnelly, T., Francheteau, J., Bryan, W., Robinson, P., Flower, M., Salisbury, M., et al., eds., Initial reports of the Deep Sea Drilling Project, Volumes 51–53: Washington, D.C., U.S. Government Printing Office, p. 815–821.

Graciansky, P. C. de, Poag, C. W., Cunningham, R., Jr., Loubere, P., Masson, D. G., Mazzullo, J. M., Montadert, L., Muller, C., Otsuka, K., Reynolds, L., Sigal, J., Snyder, S., Townsend, H. A., Vaos, S. P., and Waples, D., 1985, Initial reports of the Deep Sea Drilling Project, Volume 80, Part 1: Washington, D.C., U.S. Government Printing Office, 679 p.

Gradstein, F. M., 1978, Biostratigraphy of Lower Cretaceous Blake Nose and Blake-Bahama Basin foraminifers DSDP Leg 44, western North Atlantic Ocean, in Benson, W. E., Sheridan, R. E., et al., eds., Initial reports of the Deep Sea Drilling Project, Volume 44: Washington, D.C., U.S. Government Printing Office, p. 663–701.

Gradstein, F. M., Agterberg, F. P., Ogg, J. G., Hardenbol, J., van Veen, P., Thierry, J., and Huang, Z., 1994, A Mesozoic time scale: Journal of Geophysical Research, v. 99, p. 24051–24074.

Haq, B. U., Hardenbol, J., and Vail, P. R., 1987, Chronology of fluctuating sea levels since the Triassic (250 million years to Present): Science, v. 235, p. 1156–1167.

Harland, W. B., Cox, A. V., Llewellyn, P. G., Pickton, C. A. G., Smith, A. G., and Walters, R., 1982, A geologic time scale: Cambridge, United Kingdom, Cambridge University Press, 131 p.

Harland, W. B., Armstrong, R. L., Cox, A. V., Craig, L. E., Smith, A. G., and Smith, D. G., 1989, A geologic time scale 1989: Cambridge, United Kingdom, Cambridge University Press, 263 p.

Hays, J. D., and Pitman, W. C., III, 1973, Lithospheric plate motion, sea level changes and climatic and ecologic consequences: Nature, v. 246, p. 18–22.

Heller, P. L., Anderson, D. L., and Angevine, C. L., 1996, Is the middle Cretaceous pulse of rapid sea-floor spreading real or necessary?: Geology, v. 24, p. 491–494.

Hess, J., Bender, M. L., and Schilling, J -G., 1986, Evolution of the ratio of strontium-87 to strontium-86 in seawater from Cretaceous to present: Science, v. 231, p. 979–984.

Hodell, D. A., Mueller, P. A., McKenzie, J. A., and Mead, G. A., 1989, Strontium isotope stratigraphy and geochemistry of the late Neogene ocean: Earth and Planetary Science Letters, v. 92, p. 165–178.

Hodell, D. A., Mueller, P. A., and Garrido, J. R., 1991, Variation in the strontium isotope composition of seawater during the Neogene: Geology, v. 19, p. 24–27.

Huber, B. T., Hodell, D. A., and Hamilton, C. P., 1995, Mid- to Late Cretaceous climate of the southern high latitudes: Stable isotopic evidence for minimal equator-to-pole thermal gradients: Geological Society of America Bulletin, v. 107, p. 1164–1191.

Ingram, B. L., and Richter, F. M., 1994, Strontium isotopes in mid-Cretaceous seawater: Reply: Science, v. 266, p. 1586.

Ingram, B. L., Coccioni, R., Montonari, A., and Richter, F. M., 1994, Strontium isotopic composition of mid-Cretaceous seawater: Science, v. 264, p. 546–550.

Jenkyns, H. C., 1980, Cretaceous anoxic events: From continents to oceans: Geological Society of London Journal, v. 137, p. 171–188.

Jenkyns, H. C., Paull, C. K., Cummins, D. I., and Fullagar, P. D., 1995, Strontium-isotope stratigraphy of Lower Cretaceous atoll carbonates in the Mid-Pacific Mountains, in Winterer, E. L., Sager, W. W., Firth, J. V., and Sinton, J. M., eds., Proceedings of the Ocean Drilling Program, Scientific results, Volume 143: College Station, Texas, Ocean Drilling Program, p. 89–97.

Jeremiah, J., 1996, A proposed Albian to lower Cenomanian nannofossil biozonation for England and the North Sea Basin: Journal of Micropaleontology, v. 15, p. 97–129.

Jones, C. E., and Jenkyns, H. C., 1995, Mesozoic seawater Sr-isotope excursions link pulses of ocean-crust production to "Oceanic Anoxic Events": Eos (Transactions, American Geophysical Union), v. 76, p. 173.

Jones, C. E., Jenkyns, H. C., and Hesselbo, S. P., 1994a, Strontium isotopes in Early Jurassic seawater: Geochimica et Cosmochimica Acta, v. 58, p. 1285–1301.

Jones, C. E., Jenkyns, H. C., Coe, A. L., and Hesselbo, S. P., 1994b, Strontium isotopic variations in Jurassic and Cretaceous seawater: Geochimica et Cosmochimica Acta, v. 58, p. 3061–3074.

Keupp, H., and Mutterlose, J., 1994, Calcareous phytoplankton from the Barremian/Aptian boundary interval in NW Germany: Cretaceous Research, v. 15, p. 739–763.

Koepnick, R. B., Denison, R. E., Burke, W. H., Hetherington, E. A., Nelson, H. F., Otto, J. B., and Waite, L. E., 1985, Construction of the seawater $^{87}Sr/^{86}Sr$ curve for the Cenozoic and Cretaceous: Supporting data: Chemical Geology, v. 58, p. 55–81.

Kominz, M. A., 1984, Ocean ridge volumes and sea level change: An error analysis, in Schlee, J. S., ed., Interregional unconformities and hydrocarbon accumulation: American Association of Petroleum Geologists Memoir 36, p. 109–127.

Krasheninnikov, V. A., and Basov, I. A., 1983, Stratigraphy of Cretaceous sediments of the Falkland Plateau based on planktonic foraminifers, Deep Sea Drilling Project, Leg 71, in Ludwig, W. J., Krasheninnikov, V. A., et al., eds., Initial reports of the Deep Sea Drilling Project, Volume 71: Washington, D.C., U.S. Government Printing Office, p. 789–820.

Kump, L. R., 1989, Alternative modeling approaches to the geochemical cycles of carbon, sulfur, and strontium isotopes: American Journal of Science, v. 289, p. 390–410.

Larson, R. L., 1991, Latest pulse of the Earth: Evidence for a Mid-Cretaceous superplume: Geology, v. 19, p. 547–550.

Larson, R. L., 1994, Strontium isotopes in mid-Cretaceous seawater: Technical comment: Science, v. 266, p. 1584–1585.

Larson, R. L., and Kincaid, C., 1996, Onset of mid-Cretaceous volcanism by elevation of the 670 km thermal boundary layer: Geology, v. 24, p. 551–554.

Larson, R. L., and Olson, P., 1991, Mantle plumes control magnetic reversal frequency: Earth and Planetary Science Letters, v. 107, p. 437–447.

Leckie, R. M., 1984, Mid-Cretaceous planktonic foraminiferal biostratigraphy off Central Morocco, Deep Sea Drilling Project Leg 79, Sites 545 and 547, in Hinz, K., Winterer, E. L., et al., eds., Initial reports of the Deep Sea Drilling Project, Volume 79: Washington, D.C., U.S. Government Printing Office, p. 579–620.

Ludwig, K. R., Halley, R. B., Simmons, K. R., and Peterman, Z. E., 1988, Strontium-isotope stratigraphy of Enewetak Atoll: Geology, v. 16, p. 173–177.

Mahoney, J. J., Storey, M., Duncan, R. A., Spencer, K. J., and Pringle, M., 1993, Geochemistry and age of the Ontong Java Plateau, in Pringle, M. S., Sager, W. W., Sliter, W. V., and Stein, S., eds., The Mesozoic Pacific: Geology, tectonics, and volcanism: American Geophysical Union Monograph 77, p. 233–261.

McArthur, J. M., Thirlwell, M. F., Gale, A. S., Kennedy, W. J., Burnett, J. A., Mattey, D., and Lord, A. R., 1993, Strontium-isotope stratigraphy for the Late Cretaceous: A new curve, based on the English Chalk, in Hailwood, E., and Kidd, R., eds., High resolution stratigraphy: Geological Society of London Special Publication 70, p. 195–209.

McArthur, J. M., Kennedy, W. J., Chen, M., Thirlwell, M. F., and Gale, A. S., 1994, Strontium isotope stratigraphy for Late Cretaceous time: Direct numerical calibration of the Sr isotopic curve based on the US Western Interior: Palaeogeography, Palaeoclimatology, Palaeoecology, v. 108, p. 95–119.

McKenzie, J. A., Hodell, D. A., Mueller, P. A., and Mueller, D. A., 1988, Application of strontium isotopes to late Miocene–early Pliocene stratigraphy: Geology, v. 16, p. 1022–1025.

Miles, G. A., and Orr, W. N., 1980, Planktonic foraminifers from the Bermuda Rise, Deep Sea Drilling Project Legs 51, 52 and 53, in Donnelly, T., Francheteau, J., Bryan, W., Robinson, P., Flower, M., Salisbury, M., et al., eds., Initial reports of the Deep Sea Drilling Project, Volumes 51–53: Washington, D.C., U.S. Government Printing Office, p. 791–813.

Mutterlose, J., 1992, Migration and evolution patterns of floras and faunas in marine Early Cretaceous sediments of NW Europe: Palaeogeography, Palaeoclimatology, Palaeoecology, v. 94, p. 261–282.

Ogg, J. G., 1988, Early Cretaceous and Tithonian magnetostratigraphy of the Galicia Margin (ODP Leg 103), in Boillot, G., Winterer, E. L., et al., eds., Proceedings of the Ocean Drilling Program, Scientific results, Volume 103: College Station, Texas, Ocean Drilling Program, p. 659–684.

Paull, C. K., Fullagar, P. D., Bralower, T. J., and Röhl, U., 1995, Seawater ventilation of mid-Pacific guyots drilled on Leg 143, in Winterer, E. L., Sager, W. W., Firth, J. V., and Sinton, J. M., eds., Proceedings of the Ocean Drilling Program, Scientific results, Volume 143: College Station, Texas, Ocean Drilling Program, p. 231–241.

Premoli Silva, I., and Sliter, W. V., 1994, Cretaceous planktonic foraminiferal biostratigraphy and evolutionary trends from the Bottaccione Section, Gubbio, Italy: Palaeontographica Italia, v. 81, p. 2–90.

Raymo, M. E., Ruddiman, W. F., and Froelich, P. N., 1988, Influence of late Cenozoic mountain building on ocean geochemical cycles: Geology, v. 16, p. 649–653.

Richter, F. M., and DePaolo, D. J., 1988, Diagenesis and Sr evolution of seawater using data from DSDP 590B and 575: Earth and Planetary Science Letters, v. 90, p. 382–394.

Schlanger, S. O., Jenkyns, H. C., and Premoli Silva, I., 1981, Volcanism and vertical tectonics in the Pacific Basin related to global Cretaceous transgressions: Earth and Planetary Science Letters, v. 52, p. 435–494.

Schmidt, R. R., 1978, Calcareous nannoplankton from the western North Atlantic, DSDP Leg 44, in Benson, W. E., Sheridan, R. E., et al., eds., Initial reports of the Deep Sea Drilling Project, Volume 44: Washington, D.C., U.S. Government Printing Office, p. 703–730.

Siesser, W., 1980, Calcareous nannofossils: Legs 51 and 52 of Deep Sea Drilling Project, in Donnelly, T., Francheteau, J., Bryan, W., Robinson, P., Flower, M., Salisbury, M., et al., eds., Initial reports of the Deep Sea Drilling Project, Volume 51: Washington, D.C., U.S. Government Printing Office, p. 823–845.

Sugarman, P. J., Miller, K. G., Bukry, D., and Feigenson, M. D., 1995, Uppermost Campanian-Maestrichtian strontium isotopic, biostratigraphic, and sequence stratigraphic framework of the New Jersey coastal plain: Geological Society of America Bulletin, v. 107, p. 19–37.

Tarduno, J. A., Sliter, W. V., Bralower, T. J., McWilliams, M., Premoli Silva, I., and Ogg, J. G., 1989, M-sequence reversals recorded in DSDP sediment cores from the Western Mid-Pacific mountains and Magellan Rise: Geological Society of America Bulletin, v. 101, p. 1306–1316.

Tarduno, J. A., Sliter, W. V., Kroenke, L., Leckie, R. M., Mayer, H., Mahoney, J. J., Musgrave, R., Storey, M., and Winterer, E. L., 1991, Rapid formation of Ontong Java Plateau

by Aptian mantle volcanism: Science, v. 254, p. 399–403.

Taylor, R. J., 1982, Lower Cretaceous (Ryazanian to Albian) calcareous nannofossils, *in* Lord, A. R., ed., A stratigraphic index of calcareous nannofossils: Chichester, United Kingdom, Ellis Horwood, p. 40–80.

Tejada, M. L. G., Mahoney, J. J., Duncan, R. A., and Hawkins, M. P., 1996, Age and geochemistry of basement and alkalic rocks of Malaita and Sanata Isabel, Solomon Islands, southern margin of Ontong Java Plateau: Journal of Petrology, v. 37, p. 361–394.

Thierstein, H. R., 1973, Lower Cretaceous calcareous nannoplankton biostratigraphy: Abhandlungen Geologischen Bundesanstalt, v. 29, p. 3–53.

Thierstein, H. R., 1974, Calcareous nannoplankton—Leg 26 of the Deep Sea Drilling Project, *in* Davies, T. A., Luyendyk, B. P., et al., eds., Initial reports of the Deep Sea Drilling Project, Volume 26: Washington, D.C., U.S. Government Printing Office, p. 619–667.

Veizer, J., 1983, Chemical diagenesis of carbonates: Theory and application of trace element techniques, *in* Arthur, M., and Anderson, T., eds., Stable isotopes in sedimentary geology: Society of Economic Paleontologists and Mineralogists Short Course 10, p. 3-1–3-100.

Veizer, J., and Compston, W., 1974, $^{87}Sr/^{86}Sr$ composition of seawater during the Phanerozoic: Geochimica et Cosmochimica Acta, v. 38, p. 1461–1484.

Vogt, P. R., 1989, Volcanogenic upwelling of anoxic nutrient-rich water: Apossible factor in carbonate-bank/reef demise and benthic faunal extinctions: Geological Society of America Bulletin, v. 101, p. 1225–1245.

Whitechurch, H., Montigny, R., Sevigny, J., Storey, M., and Salters, V., 1992, K-Ar and ^{40}Ar-^{39}Ar ages of central Kerguelen Plateau basalts, *in* Wise, S. W., Jr., Schlich, R., et al., eds., Proceedings of the Ocean Drilling Program, Scientific Results, v. 120, College Station, TX, Ocean Drilling Program, p. 71–77.

Wiegand, G., 1984, Cretaceous nannofossils from the Northwest African Margin, Deep Sea Drilling Project Leg 79, *in* Hinz, K., Winterer, E. L., et al., eds., Initial reports of the Deep Sea Drilling Project, v. 79, Washington, D.C., U.S. Government Printing Office, p. 563–578.

Winterer, E. L., Ewing, J. I., Douglas, R. G., Jarrard, R. D., Lancelot, Y., Moberly, R. M., Moore, T. C., Jr., Roth, P. H., and Schlanger, S. O., 1973, Initial reports of the Deep Sea Drilling Project, v. 17, Washington, D.C., U.S. Government Printing Office, 930 p.

Wise, S. W., Jr., 1983, Mesozoic and Cenozoic calcareous nannofossils recovered by Deep Sea Drilling Project Leg 71 in the Falkland Plateau region, southwest Atlantic Ocean, *in* Ludwig, W. J., Krasheninnikov, V. A., et al., eds., Initial reports of the Deep Sea Drilling Project, Volume 71: Washington, D.C., U.S. Government Printing Office, p. 481–550.

Wise, S. W., Jr., and Wind, F. H., 1977, Mesozoic and Cenozoic calcareous nannofossils recovered by DSDP Leg 36 drilling on the Falkland Plateau, Southwest Atlantic sector of the Southern Ocean, *in* Barker, P., Dalziel, I. W. D., et al., eds., Initial reports of the Deep Sea Drilling Project, Volume 36: Washington, D.C., U.S. Government Printing Office, p. 269–492.